Response of Reinforced Concrete Structures to Aircraft Crash Impact

Prepared for

U.S. Nuclear Regulatory Commission
Contract NRC−02−07−006

Prepared by

T. Wilt
A. Chowdhury

Center for Nuclear Waste Regulatory Analyses
San Antonio, Texas

P.A. Cox

SouthWest Research Institute
San Antonio, Texas

September 2011

CONTENTS

FIGURES

FIGURES (continued)

FIGURES (continued)

TABLES

EXECUTIVE SUMMARY

In preparation for reviewing a license application for the proposed repository at Yucca Mountain, the U.S. Nuclear Regulatory Commission (NRC) independently analyzed the performance of important to safety (ITS) structures in the geologic repository operations area that were to be relied on to limit or prevent potential event sequences, as required in 10 CFR 63.112(e)(8). One area of importance was the performance evaluation of ITS surface structures when subject to an impact of an aircraft crash. The surface structures of the proposed repository at Yucca Mountain were to be constructed of reinforced concrete. Therefore, NRC directed the Center for Nuclear Waste Regulatory Analyses to develop the computational capability to predict damage to reinforced concrete structures caused by an aircraft crash impact.

An aircraft crash impact is a short duration dynamic load that could involve very large deformations and damage to both the reinforced concrete structure and the aircraft itself. Therefore, simulation of aircrash impact is computationally challenging. Because of this, the selection of an appropriate concrete material model and robust finite element software that is specialized for this type of analysis was the first step.

The computer code LS-DYNA was selected as the finite element code for this numerical analysis. LS-DYNA is a general purpose finite element code that is designed for large deformation, short duration dynamic (i.e., impact) analysis. LS-DYNA has several concrete material models built into the code (e.g., the pseudotensor model, soil/concrete model, Winfrith concrete model, and concrete damage model). For the analyses described in this report, the selected concrete damage model is essentially an improved version of the pseudotensor model. Each model has its specific applications and, in general, requires a different set of input parameters, some of which may not be easily obtainable from literature. The selection of the associated material parameters were partly based upon LS-DYNA recommendations. In addition, the parameters were correlated with experimental data from an explosion against a reinforced concrete wall, missiles impacting reinforced concrete panels, and a full-scale test of an F-4 aircraft striking a concrete block.

The goal of the numerical simulations and the correlation with experimental results was to show that LS-DYNA, using the appropriate concrete constitutive model and material parameters, can accurately predict the structural response of reinforced concrete walls when subject to intense blast and impact loads up to and including failure. The good correlations with experimental data indicated that the selected methodology, including how the concrete material was characterized, was able to appropriately model the impact events and increased confidence that the selected modeling approach was robust.

Two methods have been used in this report to evaluate the impact loads produced by an aircraft crashing into reinforced concrete buildings: the Riera method (Riera, 1968) and a finite element model of the aircraft. The Riera method is an analytical method of calculating impact and impulse forces on a structure due to an aircraft crash. This method uses the mass distribution, crush force, and velocity of an aircraft to compute an equivalent impact load resulting from an aircraft crashing into a structure. The results obtained demonstrated that the Riera total impulse was higher than the measured impulse, making the Riera method a conservative approach.

The second approach studied used a finite element model of the F-15E aircraft. The F-15E aircraft model mesh was developed using the smooth particle hydrodynamics (SPH) approach. An SPH mesh can undergo very large deformations while maintaining stability. Therefore, SPH

is an attractive option to utilize when modeling problems where large deformations and complete destruction is expected, and the primary mode of loading is due to mass/momentum.

LS-DYNA simulations of the F-15E aircraft impacting rigid surfaces and reinforced concrete walls were performed. For impacts into rigid surfaces, the forces the LS-DYNA simulations of the F-15E produced were compared to those the Riera method (Riera, 1968) predicted. At low impact velocities {112 m/s [367 ft/s]}, the forces LS-DYNA predicted were 33 percent lower than the Riera forces. The difference was due to the approximate crush force used in the Riera calculations. At higher impact velocities {215 m/s [705 ft/s]}, the impact forces LS-DYNA predicted were 4 percent lower than the Riera forces, inertial forces dominate, and the differences in crush force becomes less significant.

After the F-15E aircraft model rigid wall impact calculations were completed and good results obtained, impact analyses of the aircraft striking a reinforced concrete wall representative of a nuclear surface facility was conducted. For the impact analyses, two impact speeds were selected based on what was used for the rigid surface impact analyses 112 and 190 m/s [367 and 623 ft/s]. The aircraft impacted normal to the wall, with the nose directly in the center.

At an impact speed of 112 m/s [367 ft/s], the wall was not breached by the aircraft; however, substantial damage was evident from eroded elements and the effective plastic strain. Some evidence of possible cracking was indicated by the large plastic strains at the intersection with the buttresses and other areas of the wall. At this point the aircraft model had disintegrated and transferred all energy to the wall. At an impact speed of 190 m/s [623 ft/s], the results of the analysis showed that the wall was breached by the aircraft. During the impact, the wall began to fail as tensile forces caused the rear face rebar to break and concrete elements were deleted due to excessive plastic strain. When the simulation was stopped at this point in time, there was still significant motion of the wall; therefore, it was expected that large pieces of the wall would break off, yielding a larger breach area.

REFERENCE

Riera, J.D. “On the Stress Analysis of Structures Subjected to Aircraft Crash on Building Structures.” *Nuclear Engineering and Design*. Vol. 8. pp. 415–426. 1968.

ACKNOWLEDGMENTS

This knowledge capture report was prepared under Contract No. NRC–02–07–006 to document a detailed overview of the work performed by the Center for Nuclear Waste Regulatory Analyses (CNWRA®) for the U.S. Nuclear Regulatory Commission (USNRC) under Contract No. NRC–02–02–012. The activities reported here were performed on behalf of the USNRC Office of Nuclear Material Safety and Safeguards, Division of High-Level Waste Repository Safety. The report is an independent product of CNWRA and does not necessarily reflect the views or regulatory position of USNRC. The authors would like to thank B. Dasgupta for the technical review and B. Sagar for the programmatic review. The authors also appreciate A. Ramos for providing word processing support and L. Mulverhill for editorial support in preparation of this document.

QUALITY OF DATA, ANALYSES, AND CODE DEVELOPMENT

DATA: All CNWRA-generated original data contained in this report meet the quality assurance requirements described in the Quality Assurance Manual. Data used in this report are primarily experimental observations obtained from other publicly available sources. Each data source is cited in this report and should be consulted for determining the level of quality for those cited data. The work presented in this report is documented in Scientific Notebooks 702 and 776 (Ghosh, et al., 2008; Wilt, et al., 2009).

ANALYSES AND CODES: The finite element analyses presented in this report were conducted using ANSYS LS-DYNA, Version 10.0 (ANSYS, Inc., 2005). The version of LS-DYNA included with this software is Mpp970 (Livermore Software Technology Corporation, 2003). This version of the software is suitable for parallel processing and has been brought under CNWRA configuration control under Technical Operating Procedure–018, Development and Control of Scientific and Engineering Software. To date the software has been used only for configuration management and for the development of analysis capabilities. Spreadsheet calculations were accomplished using Microsoft® Excel® (Microsoft® Corporation, 2002).

REFERENCES

ANSYS, Inc. "ANSYS LS-DYNA." Version 10.0. Canonsburg, Pennsylvania: ANSYS, Inc. 2005.

Ghosh, A., J. Mathis, and P.A. Cox. "Impact Analyses of Aircraft Crashing into the Proposed Facilities at the Potential Repository at Yucca Mountain." Scientific Notebook No. 702. San Antonio, Texas: Center for Nuclear Waste Regulatory Analyses. 2008.

Livermore Software Technology Corporation. "LS-DYNA Keyword Users Manual." Version 970. Livermore, California: Livermore Software Technology Corporation. April 2003.

Microsoft® Corporation. "Microsoft Excel 2002.5P3." Redmond, Washington: Microsoft Corporation. 2002.

Wilt, T., J. Mathis, and P.A. Cox. "Impact Analyses of Aircraft Crashing into Structures Using ANSYS/LS-DYNA Computer Code Package in 8-Node Cluster." Scientific Notebook No. 776. San Antonio, Texas: Center for Nuclear Waste Regulatory Analyses. 2009.

1 INTRODUCTION

This report was prepared as part of the knowledge management activities for the U.S. Nuclear Regulatory Commission (NRC) high-level waste repository safety program. This report summarizes the work performed in developing the computational capabilities to simulate aircraft crash into reinforced concrete structures. The report is based on existing reports developed during prelicensing activities (Cox, et al., 2007, 2006, 2005). In addition, the report incorporates some additional aircraft crash simulations using input data and an LS-DYNA aircraft model documented in previous reports (i.e., Cox, et al., 2007, 2006, 2005).

1.1 Background

The Center for Nuclear Waste Regulatory Analyses (CNWRA®) staff began the process of developing the computational capabilities to simulate aircraft crashing into reinforced concrete structures in 2005. A report by Cox, et al. (2005) documented progress made in selecting appropriate material damage models for reinforced concrete under impact loads. Additionally, the report compared experimental observations of high explosive detonation and impact by simulated missiles on concrete walls with the numerical simulation results. The analysis resulted in the selection of a concrete damage model available in the finite element code LS-DYNA with appropriate erosion capabilities for modeling aircraft impacting a concrete structure.

The numerical simulation results were compared with published results, and the comparisons showed good correlation between measurements and calculated results. The good correlation indicated that the methodology, including how the material is characterized, was able to appropriately model aircraft crash events.

A second report by Cox, et al. (2006) continued to develop the CNWRA's computational capabilities, which involved (i) refinements of the concrete damage model characterization, (ii) structural modeling of an engine simulant representing a GE J79 aircraft engine, and (iii) evaluation of the Riera method (Riera, 1968) for calculating impact forces. The results of this study determined (i) the adequacy of the engine simulant finite element model and (ii) the appropriate selection of material parameters to characterize the response of reinforced concrete structures under impact loading. Again, correlation of numerical simulation results with experimental observations allowed refinements in the values of the concrete damage model parameters. Finally, the Riera method was used to compute impact loads on a structure by an aircraft crash. It was determined that the Riera method is conservative.

The main objective of a final report by Cox, et al. (2007) was to determine the impact forces as a result of an F-15 aircraft striking a rigid wall. In this report, two approaches were used: (i) equivalent impact loads were calculated using the Riera method (Riera, 1968) and (ii) a finite element and a smoothed particle hydrodynamics model of the F-15 aircraft was developed. This report found that the overall impact force results for both methods showed reasonable agreement. Also, the impulse force the Riera method calculated and that produced from the LS-DYNA model of the F-15 aircraft analysis compared well overall. It was concluded that the preliminary full-scale impact simulation using the aircraft smoothed particle hydrodynamics and finite element model showed a promising path forward for the study of aircraft impact scenarios.

1.2 Current Need for Aircraft Crash Simulation Capabilities

The assessment of both commercial and military aircraft crash hazards and their impact on nuclear and other critical facilities continues to be important to the owners of these facilities and many federal government agencies.

In preparation for reviewing a license application for the proposed repository at Yucca Mountain, NRC conducted independent analyses of the performance of important to safety (ITS) structures in the geologic repository operations area that were to be relied on to limit or prevent potential event sequence, as required in 10 CFR 63.112(e)(8). One area of importance was the performance evaluation of ITS surface structures when subject to an impact of an aircraft crash. The surface structures of the proposed repository at Yucca Mountain were to be constructed of reinforced concrete. Therefore, NRC directed the CNWRA to develop the computational capability to predict damage to reinforced concrete structures caused by an aircraft crash impact.

On September 11, 2001, terrorists simultaneously attacked the World Trade Center in New York City, New York, and the Pentagon in Washington, DC, utilizing large commercial aircraft as weapons, which caused widespread loss of life and destruction of property.

These incidents have drawn special attention from the public, industry groups such as the Nuclear Energy Institute (NEI), and federal government agencies such as the National Institute of Standards and Technology (NIST) and NRC.

NRC has determined that it is prudent for nuclear power plant designers to rigorously account for the potential effects of an impact of a large, commercial aircraft. In the Federal Register (74 FR 28111; June 12, 2009), effective July 13, 2009, NRC issued a final rule that will require applicants for new nuclear power reactors to perform an assessment of the effects of the impact of a large commercial aircraft. As stated in the Federal Register (74 FR 28111; June 12, 2009), the technical issues related to aircraft impact assessment should include the following damage mechanisms: (i) structural response, (ii) shock and vibration effects, and (iii) fire effects of the aircraft impact. The structural analysis should evaluate both local and global plantwide response. Also specified in the Federal Register (74 FR 28111; June 12, 2009), "the structural assessment is to be based on a detailed model of the plant accounting for nonlinear material and geometric behavior."

As a result of the ruling, regulations in 10 CFR Part 50 were amended to include section 10 CFR 50.150, Aircraft Impact Assessment. In particular, 10 CFR 50.150(a) specifies that "the applicant shall identify and incorporate into the design those design features and functional capabilities to show that, with reduced use of operator actions: (i) The reactor core remains cooled, or the containment remains intact; and (ii) spent fuel cooling or spent fuel pool integrity is maintained."

Subsequently, NRC issued Draft Regulatory Guide DG–1176 (NRC, 2009). The guide sets forth a method that NRC considers acceptable for satisfying the regulations in 10 CFR 50.150. Specifically, this draft guide endorses the aircraft impact assessment methodologies described in the NEI's report 07-13 (NEI, 2009). It is the NRC position that conformance with guidance described in NEI 07-13 is an acceptable method for satisfying the regulatory requirements in 10 CFR 50.150(a), which pertains to the assessment of aircraft impacts for new nuclear power reactors (NRC, 2009).

NEI 07-13 (NEI, 2009) states that for containment structures and spent fuel pools, two structural failure modes need to be evaluated: (i) local failure characterized by scabbing and perforation due to impact of the aircraft engines and (ii) global failure in the form of plastic collapse due to impact of the entire aircraft. One approach for determining both local and global structural failure is the explicit modeling of the aircraft, the target (e.g., a building), and the simulation of the aircraft crashing into the structure. As discussed in Section 1.1, the CNWRA has developed the computational capabilities to perform this type of analysis.

The analyses reported in this report were performed for application to surface structures handling high-level waste and spent-fuel of a repository site. The analyses were generic in nature and no effort was made to relate those to nuclear power plants or spent fuel pools.

In addition to performing a local and global structural analysis, it is also necessary to evaluate the effects of fire and shock that can cause damage to important systems utilized for fuel cooling. For fire and shock damage, important considerations are (i) effects of a large fire outside the containment and effects of fire inside any adjacent buildings below the point of impact and (ii) shock damage to fragile structures, systems, and components directly attached to the containment wall. If the structural analyses indicate perforation of the containment boundary, then fire and physical damage inside the containment must be considered.

1.3 Objective and Scope

The objective of this report is to present a detailed overview of the work the CNWRA performed (Cox, et al., 2007, 2006, 2005) to develop the ability to computationally simulate and analyze the effects of an aircraft crashing into reinforced concrete structures. The particular finite element software chosen for this work was LS-DYNA (Livermore Scientific Technology Corporation, 2003a,b). The CNWRA has used LS-DYNA in past programs for NRC to solve problems that involve high rate loading and material failure. The code has undergone verification and validation testing by the CNWRA.

1.4 Organization of the Report

Chapter 2 discusses the characterization of the selected LS-DYNA concrete model using experimental data and the results of impact experiments using both rigid and deformable missiles against reinforced concrete walls. Chapter 3 details the Riera method (Riera, 1968) and evaluates its accuracy for predicting impact loads. Chapter 4 discusses the development of a smoothed particle hydrodynamics model of an F-15E aircraft. Chapter 5 compares the impact forces on a rigid surface produced by the Riera method and the F-15E smooth particle hydrodynamics (SPH) model. Chapter 6 details a full-scale impact simulation of the F-15E SPH model striking a reinforced concrete wall. Finally, Chapter 7 provides a summary and conclusions for the report.

2 MATERIAL MODELING OF CONCRETE

2.1 LS-DYNA Concrete Damage Model

The LS-DYNA explicit finite element program has several concrete material models available (e.g., the pseudotensor model, soil/concrete model, Winfrith concrete model, and a concrete damage model) (Livermore Software Technology Corporation, 2003b). Each model was developed for a specific application and requires a different set of input parameters. In general, the values of the necessary material parameters cannot always be found in the literature. The aircraft crash impact analyses presented in this report utilized the LS-DYNA concrete damage model (keyword *MAT_CONCRETE_DAMAGE) Malvar, et al. (1997) formulated, which is an improved version of the pseudotensor model.

The concrete damage model Malvar, et al. (1997) developed is a three-invariant plasticity model that accounts for changes in yield stress as a function of plastic strain. The specific forms of the invariants used in the model are $I_1 = (\sigma_1 + \sigma_2 + \sigma_3)$, which is the first invariant of the total stress tensor; $J_2 = [(s_1^2 + s_2^2 + s_3^2)/2]$, which is the second invariant of the deviatoric stress tensor where $s_1,\ s_2,\ s_3$ are principal deviatoric stresses; and $J_3 = s_1 s_2 s_3$, which is the third invariant of the deviatoric stress tensor. Note that including I_1 accounts for pressure dependence. As with conventional J_2-plasticity, J_2 enters the yield function and the specific form of the yield function defines the yield surface. The third invariant, J_3, is used to calculate the Lode angle (Chen, 2007), which modifies the shape of the failure surface in the deviatoric plane. Including J_3 is commonly used for materials such as concrete, which have a triangular-shaped failure surface.

The deviatoric stress used in the second and third invariants is limited by the function $\Delta\sigma(y, m, r)$ defined by linear relationships of three failure surfaces that are functions of pressure: (i) yield surface, $\Delta\sigma_y$; (ii) maximum failure surface, $\Delta\sigma_m$; and (iii) residual failure surface, $\Delta\sigma_r$,

$$\Delta\sigma_y = a_{0Y} + \frac{P}{a_{1Y} + a_{2Y}P} \tag{2-1}$$

$$\Delta\sigma_m = a_0 + \frac{P}{a_1 + a_2 P} \tag{2-2}$$

$$\Delta\sigma_r = \frac{P}{a_{1f} + a_{2f}P} \tag{2-3}$$

in which P (pressure) is defined by $I_1/3$. As normally defined in standard plasticity, the yield surface determines the stress state at which plasticity first occurs. The yield surface then increases until it reaches the maximum failure surface, which defines the upper limit on the stress. Once the stress passes the upper limit, the concrete material begins to soften until the residual failure surface is reached. Thus, these surfaces are defined by eight material parameters: $a_{0Y}, a_{1Y}, a_{2Y}, a_0, a_1, a_2, a_{1f}, a_{2f}$.

The parameter a_0 represents the maximum failure strength when the pressure, P, is zero and a_0 is defined by $f_c'/4$ where f_c' is the compressive strength of the concrete. The parameter a_1 has been assigned a value of 1/3, and a_2 is defined as $1/f_c'$. All of these parameter values were

taken from the *MAT_PSEUDO_TENSOR model given in the LS-DYNA Keyword User's Manual (Livermore Software Technology Corporation, 2003a).

In addition, the initial yield strength $\Delta\sigma_y$ is estimated by the following equation:

$$\Delta\sigma_y = 0.45\Delta\sigma_m = 0.45\left(a_0 + \frac{P}{a_1 + a_2 P}\right) \tag{2-4}$$

Recall that the parameters a_0, a_1, a_2 were previously determined. The parameters a_{0Y}, a_{1Y}, a_{2Y} are then obtained from a graphical fit to the initial yield surface, which is determined from triaxial compression tests of plain concrete. Malvar, et al. (1997) detail the procedure for determining these parameters.

For the residual failure surface parameters, a_{1f}, a_{2f}, the parameter a_{1f} was assigned a value of 0.385 as suggested in the *MAT_PSEUDO_TENSOR model given in the LS-DYNA Keyword User's Manual (Livermore Software Technology Corporation, 2003a). The term a_{2f} is obtained from an experimentally determined failure surface. Again, Malvar, et al. (1997) detail the procedure for determining this parameter.

In addition, damage accumulation is defined by the parameters b_1, b_2, b_3. The concrete model's damage is separated into shear (deviatoric) and volumetric components. The parameters b_1, b_2 are associated with shear damage accumulation, and the parameter b_3 is associated with volumetric damage. For brevity, the lengthy equations used to calculate b_1, b_2, b_3 are not presented here; however, all details for obtaining these parameters are given in Malvar, et al. (1997). All required material parameters and their values used in the analyses presented in this report are summarized in Table 2-1.

Additional details of the selection of the material parameters listed in Table 2-1 are given in Cox, et al. (2005).

The current failure surface is defined using linear interpolation between the two active failure surfaces. After reaching the initial yield surface, yet below the maximum surface, the active failure surface is defined as

$$\Delta\sigma = \eta\left(\Delta\sigma_m - \Delta\sigma_y\right) + \Delta\sigma_y \tag{2-5}$$

After the maximum failure surface has been reached, the concrete material begins to soften. The active failure surface is then determined by linearly interpolating between the maximum failure surface and the residual failure surface; that is,

$$\Delta\sigma = \eta(\Delta\sigma_m - \Delta\sigma_r) + \Delta\sigma_r \tag{2-6}$$

The material parameter η in Eqs (2-5) and (2-6) is defined as the damage function, which is expressed in terms of user-defined pairs (η, λ) where the term λ is the accumulated effective plastic strain.

The damage function increases to a value of one, which corresponds to the concrete's maximum strength, and then decreases (i.e., softens) to a value of zero, which corresponds to the concrete's residual strength. The damage function, $\eta(\lambda)$, is given in Table 2-2. The values

Table 2-1. List of Concrete Model Input Parameters	
Material Parameter	**Value**
ρ, kg/m^3 [lb/ft^3] Mass Density	2,300 [144]*
v, Poisson's Ratio	0.19†
f'_c, Pa [psi] Compressive Strength of Concrete	2.35 × 107 [3,408]*
a_0, Pa [psi] Cohesion	5.88 × 106 [853]‡
a_1, Pressure Hardening Coefficient	0.333‡
a_2, Pressure Hardening Coefficient	1.42×10^{-8}‡
a_{0Y}, Pa [psi] Cohesion for Yield	2.64 × 106 [383]§
a_{1Y}, Pressure Hardening Coefficient for Yield Limit	0.75§
a_{2Y}, Pressure Hardening Coefficient for Yield Limit	3.10×10^{-8}§
a_{1F}, Pressure Hardening Coefficient for Failure	0.39§
a_{2F}, Pressure Hardening Coefficient for Failure	1.39×10^{-8}§
b_1, Damage Scaling Factor	1.250‡
b_2, Damage Scaling Factor for Uniaxial Tension	4.0§
b_3, Damage Scaling Factor for Triaxial Tension	10.0§

*Wang, C.K. and C.G. Salmon. *Reinforced Concrete Design*. 5th Edition. New York City, New York: Harper-Collins. 1992.
†MacGregor, J.G. and H.K. Wright. *Reinforced Concrete Mechanics and Design*. 4th Edition. Upper Saddle River, New Jersey: Prentice Hall. 2005.
‡Livermore Software Technology Corporation. "LS-DYNA Keyword User's Manual." Version 970. Livermore, California: Livermore Software Technology Corporation. April 2003.
§Malvar, L.J., J. Crawford, J. Wesevich, and D. Simons. "A Plasticity Concrete Material Model for DYNA3D." *International Journal of Impact Engineering*. Vol. 19, Nos. 9–10. pp. 847–873. 1997.

Table 2-2. Damage Function Values	
Effective Plastic Strain	**Damage Scale Factor**
λ	η(λ)
0	0.309
8.62×10^{-6}	0.543
2.15×10^{-5}	0.840
3.14×10^{-5}	0.975
3.95×10^{-4}	1.0
5.17×10^{-4}	0.79
6.38×10^{-4}	0.63
7.98×10^{-4}	0.469
9.67×10^{-4}	0.383
1.41×10^{-3}	0.247
1.97×10^{-3}	0.173
2.59×10^{-3}	0.136
0.909	0

listed in Table 2-2 are those suggested from the *MAT_PSEUDO_TENSOR model described in the LS-DYNA Keyword User's Manual (Livermore Software Technology Corporation, 2003a).

In addition to the material parameters for the concrete damage model, an equation of state is needed to describe the pressure-compaction curve representing the volumetric response behavior of the concrete. The tabulated compaction model was chosen, and values for the model were determined from a procedure found in the Winfrith concrete material model (*MAT_WINFRITH_CONCRETE) description in the LS-DYNA Keyword User's Manual

(Livermore Software Technology Corporation, 2003a). If a pressure-compaction response curve specific to the concrete being modeled cannot be obtained from experimental data, the *MAT_WINFRITH_CONCRETE model description in the LS-DYNA Keyword User's Manual suggests a method for developing a compaction curve.

First, pressure is defined as positive in compression, and volumetric strain is defined as the natural log of the relative volume, which is negative in compression. The compaction curve data are input in a tabular format and given in order of increasing compression with no initial zero point (Livermore Software Technology Corporation, 2003a). The LS-DYNA recommended values of the pressure-compaction response curve are shown in Table 2-3.

In Table 2-3, the parameters p_1 and K are defined by the following expressions. p_1, the pressure at uniaxial compressive failure, is given as

$$p_1 = \frac{f_c'}{3} \tag{2-7}$$

where f_c' is the concrete's unconfined compressive strength. The bulk modulus K is given as

$$K = \frac{E_s}{3(1-2\nu)} \tag{2-8}$$

where E_s is one-half the tangent modulus for the concrete and ν is Poisson's ratio for the concrete.

In addition to the concrete damage model, element erosion was used to simulate concrete breakup. Erosion was used to simulate, in a qualitative sense, representation of concrete scabbing and spalling effects. Element erosion was activated by using the *MAT_ADD_EROSION option as described in the LS-DYNA Keyword User's Manual (Livermore Software Technology Corporation, 2003a). Elements that reach a user-specified failure strain are deleted from the analysis. A parametric study was performed, which consisted of running numerical simulations with different erosion strain values and observing overall damage. Based on this study, an erosion failure strain parameter of 0.5 was selected.

Table 2-3. Volumetric Strain Versus Pressure

Volumetric Strain	Pressure (MPa)
$-p_1/K$	1.00 × p_1
−0.002	1.50 × p_1
−0.004	3.00 × p_1
−0.010	4.80 × p_1
−0.020	6.00 × p_1
−0.030	7.50 × p_1
−0.041	9.45 × p_1
−0.051	11.55 × p_1
−0.062	14.25 × p_1
−0.094	25.05 × p_1

2.2 Application of LS-DYNA Concrete Damage Model for Impact Simulations

As discussed in Section 2.1, the selection of some of the material parameters was based upon values taken from different references. Cox, et al. (2005) presented details of using LS-DYNA to simulate impact loading on reinforced concrete panels using small-, intermediate-, and full-scale idealized aircraft engine models. The results of the LS-DYNA simulations were compared with experiments Muto, et al. (1989a,b) and Esashi, et al. (1989) conducted.

The impact tests of Muto, et al. (1989a,b) and Esashi, et al. (1989) were based on the GE J79 engine used in the F-4 Phantom fighter aircraft. Dimensions of the GE J79 engine and the simplified models used in the tests are given in Muto, et al. (1989a,b) and Esashi, et al. (1989). As an example, Figure 2-1 shows the actual GE J79 engine and its corresponding simulant used in the full-scale tests of Muto, et al. (1989b).

These GE J79 engine simulants were used in impact experiments involving reinforced concrete panels of different thicknesses supported at the corners with steel backup plates. Additional details of the reinforced concrete panel, such as width, height, and reinforcement steel placement, are given in Cox, et al. (2005); Muto, et al. (1989a,b); and Esashi, et al. (1989).

Depending on the scale of the idealized engine, the experiments were performed at impact speeds of 215, 150 m/s, and 100 m/s [705, 492, and 328 ft/s]. The experimental results of Muto, et al. (1989a,b) and Esashi, et al. (1989) described the physical damage to the concrete wall produced by the engine impacts. Additional details of the panel thickness, engine weight, and the velocities used in the different tests are shown in Tables 2-4, 2-5, and 2-6.

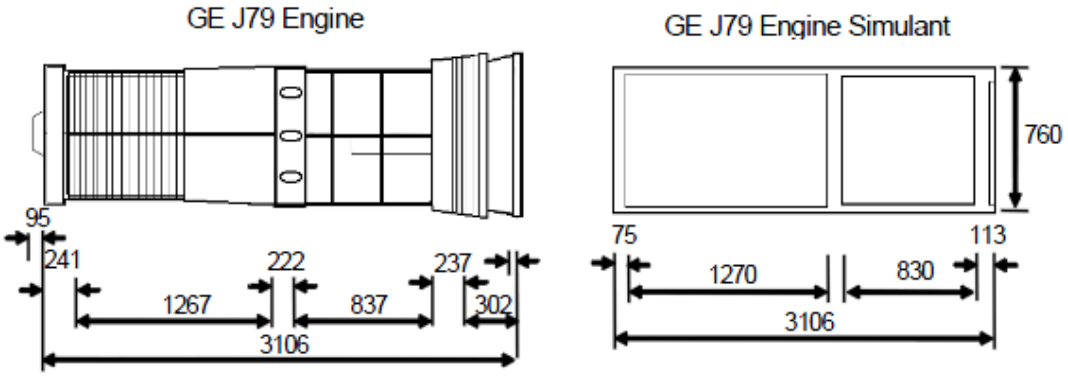

Figure 2-1. Idealized Engine Model of GE J79 Engine Used in Finite Element Simulation of Full-Scale Test (Muto, et al., 1989b)
(All Dimensions Are Given in mm; 25.4 mm = 1 in)

Table 2-4. LS-DYNA Results and Comparison With Experiments:* Small-Scale (1/7.5 Scale) Idealized GE-J79 Engine				
Wall Thickness	**Engine Weight**	**Engine Velocity**	**Observed Damage Mode**	**LS-DYNA Results**
12 cm [4.72 in]	3.5 kg [7.72 lb]	215 m/s [705 ft/s]	Perforation	Perforation
		150 m/s [492ft/s]	Scabbing	Scabbing
		100 m/s [328ft/s]	Penetration	Penetration

*Muto, K., H. Tachikawa, T. Sugano, H. Tsubota, H. Kobayashi, Y. Kasai, N. Koshika, and T. Tsujimoto. "Experimental Studies on Local Damage of Reinforced Concrete Structures by the Impact of Deformable Missiles, Part 1: Outline of the Test Program and Small-Scale Tests." Transaction of the 10th International Conference on Structural Mechanics in Reactor Technology (SMiRT 10), Anaheim, California, August 14–19, 1989. Los Angeles, California: American Association for Structural Mechanics in Nuclear Reactors. 1989.

Table 2-5. LS-DYNA Results and Comparison With Experiments:* Intermediate-Scale (1/2.5 Scale) Idealized GE-J79 Engine				
Wall Thickness	**Engine Weight**	**Engine Velocity**	**Observed Damage Mode**	**LS-DYNA Results**
35 cm [14 in]	100 kg [221 lb]	215 m/s [705 ft/s]	Perforation	Perforation
45 cm [18 in]		215 m/s [705 ft/s]	Scabbing	No Scabbing†
45 cm [18 in]		250 m/s [820 ft/s]	Just Perforation	Just Perforation

*Esashi, Y., H. Ohnuma, C. Ito, and K. Shirai. "Experimental Studies on Local Damage of Reinforced Concrete Structures by the Impact of Deformable Missiles, Part 2: Intermediate-Scale Tests." Transaction of the 10th International Conference on Structural Mechanics in Reactor Technology (SMiRT 10), Anaheim, California, August 14–19, 1989. Los Angeles, California: American Association for Structural Mechanics in Nuclear Reactors. 1989.
†However, there was significant penetration.

Table 2-6. LS-DYNA Results and Comparison With Experiments:* Full-Scale Idealized GE-J79 Engine				
Wall Thickness	**Engine Weight**	**Engine Velocity**	**Observed Damage Mode**	**LS-DYNA Results**
160 cm [63 in]	1,463 kg [3,225 lb]	215 m/s 705 [ft/s]	Penetration	Penetration

*Muto, K., H. Tachikawa, T. Sugano, H. Tsubota, N. Nagamatsu, N. Koshika, M. Okano, K. Suzuki, and S. Ohrui. "Experimental Studies on Local Damage of Reinforced Concrete Structures by the Impact of Deformable Missiles, Part 3: Full-Scale Tests." Transaction of the 10th International Conference on Structural Mechanics in Reactor Technology (SMiRT 10), Anaheim, California, August 14–19, 1989b. Los Angeles, California: American Association for Structural Mechanics in Nuclear Reactors. 1989.

Figure 2-2 shows a representative example of an LS-DYNA finite element model of the GE J79 engine simulant.

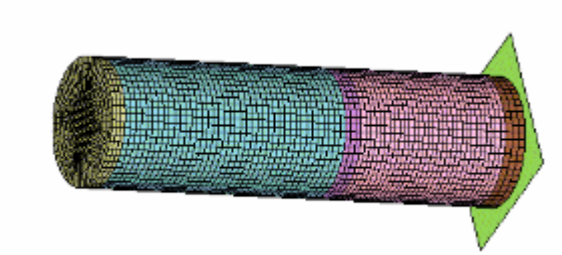

Figure 2-2. LS-DYNA Finite Element Model of Full-Scale GE J79 Engine Simulant (Cox, et al., 2006)

The GE J79 engine simulant used in the experiments of Muto, et al. (1989b) was constructed of steel. Therefore, the LS-DYNA finite element model used elastic-plastic material parameters to model the steel. Full details of the elastic-plastic material parameters used for the steel can be found in Cox, et al. (2006).

Muto, et al. (1989c) performed a displacement-controlled crush test of the full-scale engine simulant. Similarly, an LS-DYNA analysis was performed to simulate the crush test. The LS-DYNA simulation results, documented in Cox, et al. (2006), showed good agreement overall with the experimental test data of Muto, et al. (1989c). These results demonstrated that the LS-DYNA engine simulant finite element model's structural behavior was similar to that of the actual engine simulant.

The damage modes observed in the tests were classified according to Muto, et al. (1989a) in the following terms:

- Perforation mode: the engine passed through the panel completely
- Just perforation mode: perforation is just barely prevented—the engine did not pass through the panel but stuck in the panel creating a large opening with breakage of reinforcement bars
- Scabbing mode: considerable concrete debris is ejected off the back surface of the panel and may include the severe case where a small opening is created on the rear surface; and (iv) penetration mode: a crater is formed on the front face of the panel, but no damage occurs on the rear face

The LS-DYNA impact simulation results and the experimental observations of Muto, et al. (1989a,b) and Esashi, et al. (1989) are compared in Tables 2-4, 2-5, and 2-6 and Figure 2-3. The damage modes from the LS-DYNA impact simulations agree with the actual damage observed in the experiments of Muto, et al. (1989a,b) and Esashi, et al. (1989).

In addition to matching the damage modes, a quantitative comparison was made for penetration depth for the full-scale engine simulant impacting the 160-cm [63-in]-thick panel at a velocity of 215 m/s [705 ft/s]. The experimentally measured crater depth was approximately 21 cm [8.3 in] with no observed scabbing of the back surface (Muto, et al., 1989b). The approximate average depth of penetration observed in the LS-DYNA numerical simulation was 22 cm [8.7 in], and there was no back surface scabbing, which compares well with the experimental results. The crater predicted in the LS-DYNA numerical simulation is shown in Figure 2-3(d).

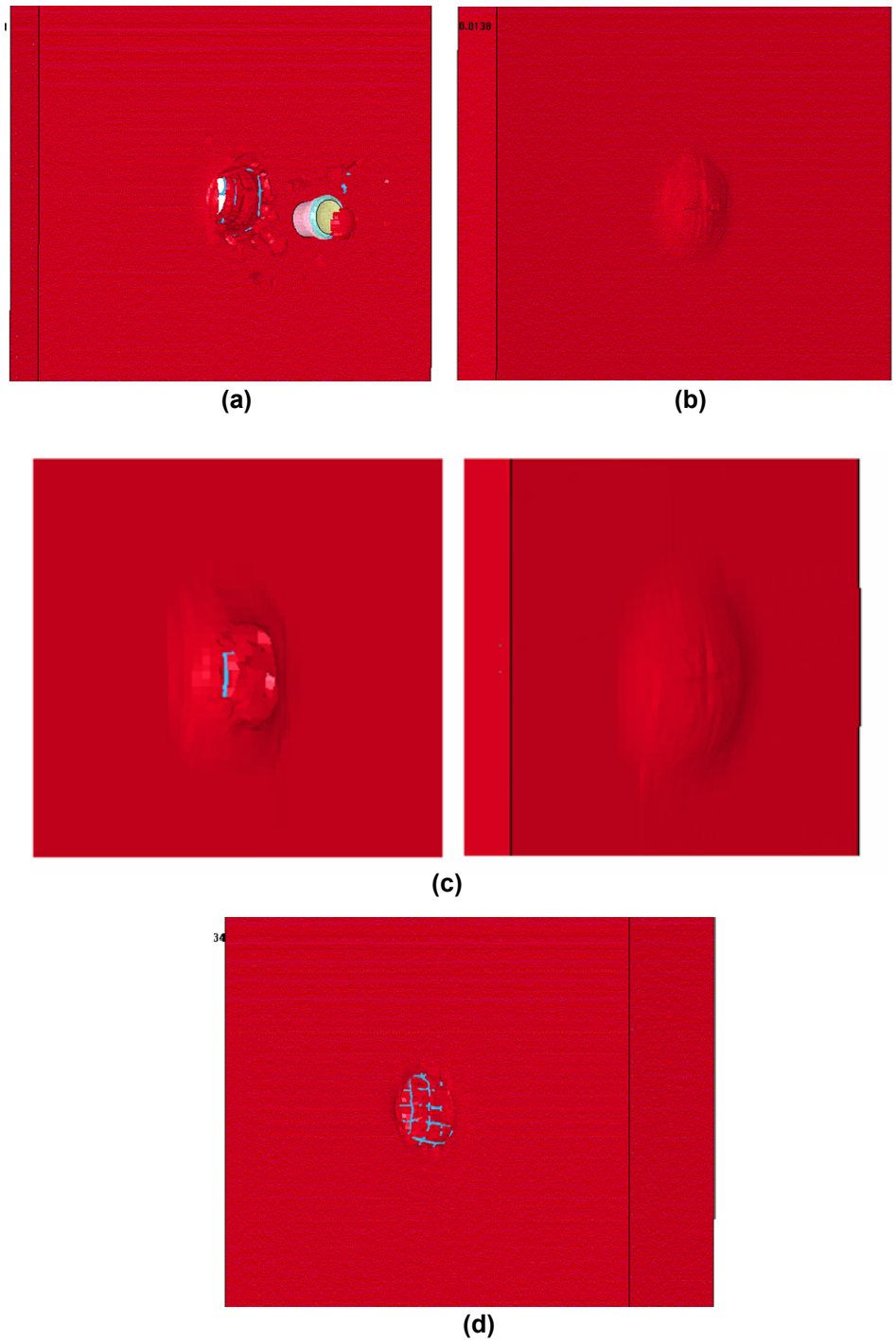

Figure 2-3. Results of LS-DYNA Simulations Showing Different Damage Modes for an Idealized Engine Striking Reinforced Concrete Panels. (a) Small-Scale Engine Impacting 12 cm [4.7-in] Thick Panel at 215 m/s [705 ft/s]: Perforation of Panel. (b) Small-Scale Engine Impacting 12-cm [4.7-in] Thick Panel at 150 m/s [492 ft/s]: Scabbing Damage at Rear of Panel. (c) Intermediate-Scale Engine Impacting 45-cm [17.7-in] Thick Panel at 215 m/s [705 ft/s] Strike (Left) and Rear (Right) Faces: Penetration Occurred at the Strike Face. (d) Full-Scale Engine Impacting 160 cm [63 in] Thick Panel at 215 m/s [705 ft/s] Strike Face: Penetration in Form of a Crater.

Backside surface displacements, located at the center of the panel, were compared using those obtained from the LS-DYNA simulation and the experiments of Muto, et al. (1989b) as shown in Figure 2-4.

Note that the LS-DYNA simulation matched measured maximum displacements in magnitude (Figure 2-4) but not in the character of the displacement history. Specifically, the LS-DYNA simulation results failed to capture the experimentally measured feature of "bounce back" where after reaching the peak displacement, the displacement rate decreases, as shown in the curve labeled "Test Data" in Figure 2-4. Therefore, the concrete damage material parameters were further refined in an attempt to improve correlation with the experimentally observed displacement history of Muto, et al. (1989b).

2.3 Refinement of LS-DYNA Concrete Damage Model Material Parameters

To refine the material parameters used in the LS-DYNA concrete damage model, additional LS-DYNA simulations were run for the case of the full-scale engine simulant impacting a 160-cm [63-in]-thick reinforced concrete panel with a velocity of 215 m/s [705 ft/s]. A sensitivity study of the concrete damage material parameters b_2 and b_3 (Table 2-1) was performed to improve the match with the experimentally measured back surface displacements. Selected results from the sensitivity study are shown in Figure 2-5.

The analysis with the concrete damage material parameters $b_2 = 15$ and $b_3 = 5$ was considered the best fit to the measured data. This selection was based upon the LS-DYNA simulation back surface displacement matching the peak magnitude of the displacement and because the simulation results now capture the experimentally observed bounce-back effect. All other concrete damage model parameters listed in Table 2-1 remain the same.

The maximum penetration depth from the LS-DYNA simulation also was compared with experimental results to investigate the effect of changes in b_2 and b_3. As discussed in Section 2.2, experimental data indicated 21 cm [8.25 in] of penetration into the front face of the concrete panel. The LS-DYNA simulation now results in a crater depth of approximately 20 cm [7.8 in], which is comparable to the test data. A cross-sectional view of the panel with the crater is shown in Figure 2-6.

Note, however, there is an offset in the LS-DYNA calculated displacement time history that begins at approximately 4 milliseconds, which is not evident in the measured displacements of Muto, et al. (1989b). Further investigation to determine the cause of this behavior was performed.

To investigate a possible cause of the offset in the calculated displacement, the tangent (hardening) modulus and the failure strain material parameters for steel, used in the LS-DYNA engine simulant model, were varied to see their effect on the calculated displacements. Based on a sensitivity study, it became apparent that the offset in the displacement time history was caused by the collapse of the front cylinder of the LS-DYNA engine simulant model. This produced a decrease in the displacement rate (i.e., penetration slowed) between approximately 4 and 8 milliseconds, after which the displacement rate resumed as the engine simulant's intermediate bulkhead impacted the panel.

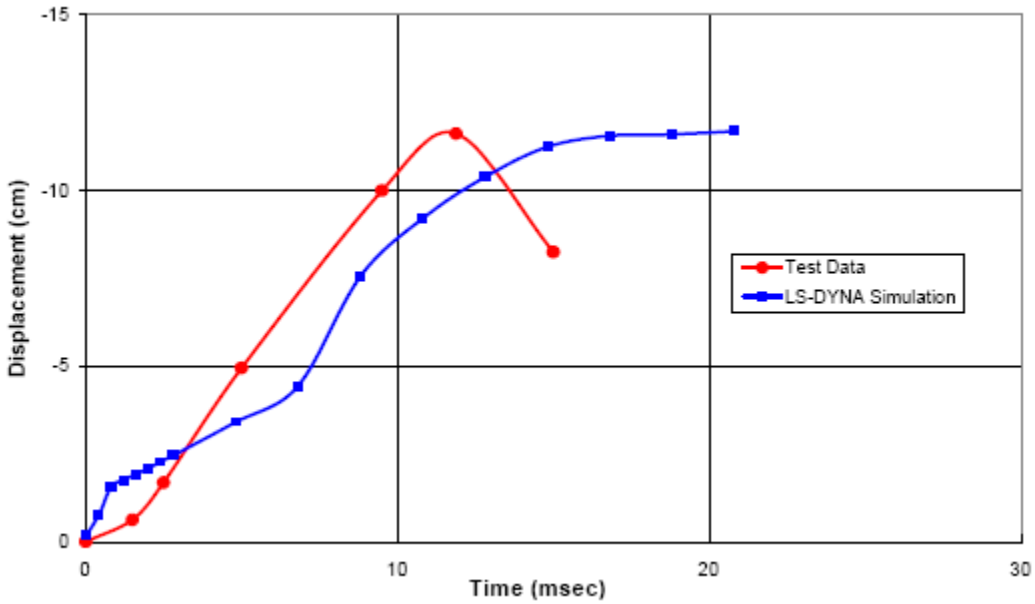

Figure 2-4. Displacement Versus Time Comparison for Full-Scale Engine Test (Muto, et al., 1989b). Displacement Measured on Backside of Test Plan [1 cm = 0.39 in].

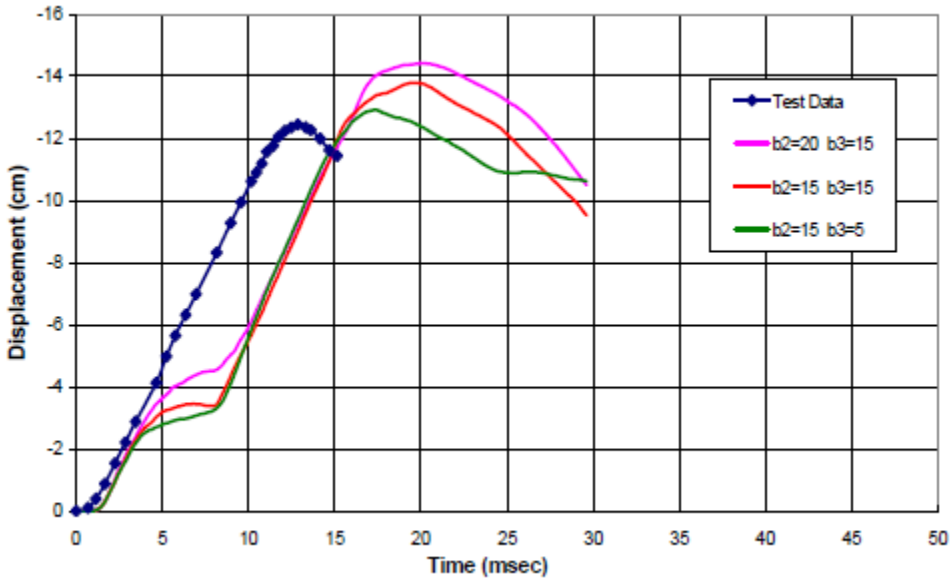

Figure 2-5. Displacement Versus Time Results for Full-Scale Panel Test (Muto, et al., 1989b). Trial Runs with Various Values of Concrete Damage Parameters b_2 and b_3 [1 cm = 0.39 in].

Figure 2-6. LS-DYNA Finite Element Results Showing Crater Depth Due to Impact of Engine Simulant [1 cm = 0.39 in]

Based on these results, there appeared to be a coupling between the concrete material parameters and the crush behavior of the LS-DYNA engine stimulant, which directly affects the structural response of the panel. At this time, additional numerical studies would be needed to further investigate the cause of the temporary decrease in the displacement rate that is now present.

3 EVALUATION OF AIRCRAFT IMPACT LOADS

3.1 Introduction

When a facility (e.g., a high-level waste repository surface facility, a spent fuel facility, etc.) is subject to impact by an aircraft (missile), the global damage is evaluated in terms of excessive deformation (i.e., displacement, or collapse of the structure).

For a global response evaluation, the target's deformation due to missile impact depends on the characteristics of the missile and the target. The important parameters for the missile are mass, stiffness, strength, size, and velocity. The important parameters for the target are geometry, support conditions, stiffness, and strength.

As given in Hossain, et al. (1997), there are three analytically based methods that can be used to evaluate global damage: (i) energy balance method, (ii) force time history analysis method, and (iii) missile target interaction analysis method.

This chapter , the focuses will be on the force time history analysis method, which is typically associated with Riera (1968). The Riera method uses the aircraft's mass, strength properties, and its velocity to determine the impact force time history. The Riera method makes two assumptions: (i) the target is rigid and (ii) the impact orientation is normal to the target so the aircraft fuselage will progressively crush/buckle axially. Hossain, et al. (1997) state that the impact orientation assumption results in the highest missile stiffness making the Riera method conservative. Thus, the damage potential of a crashing aircraft depends on the combination of the mass of the aircraft (or any hard components, such as engine or landing gear) and the speed of the impact. The critical impact speed is different for each aircraft type due to differences in the distribution of mass.

Section 3.2 will discuss the Riera method that can calculate the equivalent impact force for different types of aircraft. Section 3.3 will use results from a full-scale impact test using an F-4 aircraft to evaluate the accuracy of the Riera method for calculating the impact force. Finally, Section 3.4 will present LS-DYNA finite element analyses using experimentally measured and Riera-calculated load-time histories to evaluate the response of the concrete block target used in the full-scale F-4 aircraft impact tests.

3.2 The Riera Method

For a crashing aircraft striking a target, normal to the impact surface at time t, the impact force $F(t)$ is given by

$$F(t) = P_c[x(t)] + \mu[x(t)]v^2(t) \tag{3-1}$$

where $x(t)$ is the distance measured from the nose of the aircraft to the current location, $P_c[x(t)]$ is the load necessary to crush or deform the aircraft fuselage, $\mu[x(t)]$ is the mass per unit length of the aircraft, and $v(t)$ is the velocity of the uncrushed portion. Both $P_c[x(t)]$ and $\mu[x(t)]$ are functions of the position along the aircraft, which is usually measured from the nose.

Given known distributions for both $P_c[x(t)]$ and $\mu[x(t)]$, and the initial impact velocity, Eq. (3-1) is solved stepwise in time starting at the instant of impact to provide the impact force on a rigid

surface. For the results presented next, a Microsoft® Excel® (Microsoft Corporation, 2002) spreadsheet program was written to calculate the impact forces as a function of time.

3.3 Comparison of Riera-Calculated Impact Forces With Measured Impact Forces From a Full-Scale F-4 Crash Test

Sugano, et al. (1993) performed experiments consisting of an actual full-scale F-4 aircraft crashing into a massive concrete block. Sugano, et al. (1993) included the mass distribution and crushing force for the F-4 aircraft, which are required input for the Riera method (Riera, 1968). The test result data also included the measured impact forces generated by the F-4 aircraft striking the concrete block. To demonstrate the Riera method, the experimentally measured impact forces were compared to numerical calculations of impact forces using the Riera method.

The mass per unit length μ and crush force P_c of the F-4 aircraft were obtained directly from data Sugano, et al. (1993) reported. Both quantities, which are a function of position along the length of the aircraft, were measured from nose to tail. The mass per unit length μ and crush force P_c are shown in Figures 3-1 and 3-2, respectively. Note that the distribution of μ in Figure 3-1 is given for both the F-4 aircraft only and the F-4 aircraft in its test configuration, which included skids and rockets. Figure 3-2 shows the crush force P_c as a function of position along the aircraft, which was measured during the test. Using this experimental data, an Excel (Microsoft Corporation, 2002) spreadsheet program was written to calculate the impact forces shown in Figure 3-3 for the F-4 aircraft.

Because the experimental F-4 test of Sugano, et al. (1993) was performed at 215 m/s [705 ft/s], this same velocity was used for the comparison between measured impact forces Sugano, et al. (1993) reported and those calculated using the Riera method (Riera, 1968) discussed previously. The results of this comparison are shown in Figure 3-4.

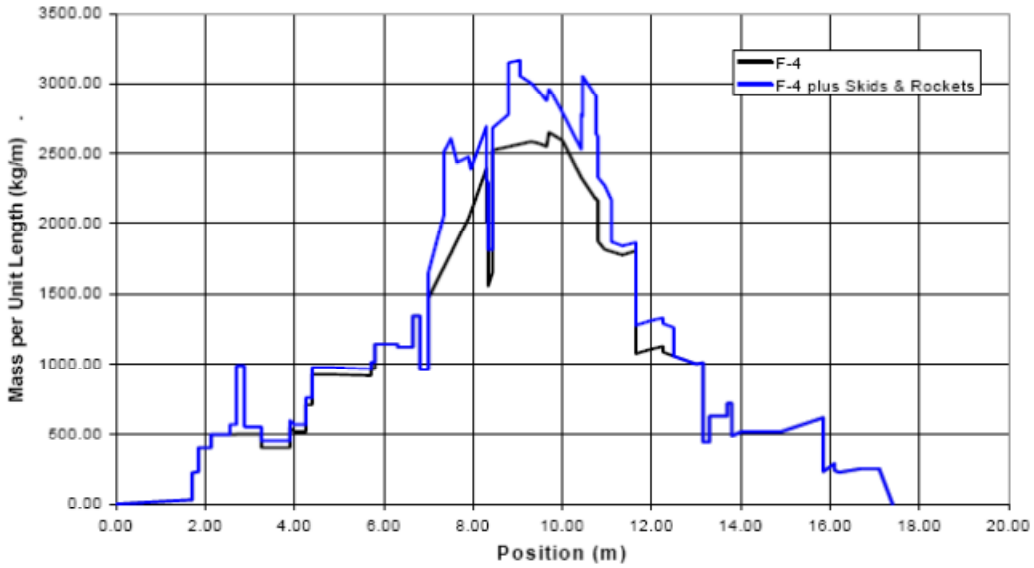

Figure 3-1. Mass Per Unit Length, μ, for the F-4 Aircraft With and Without Skids and Rockets Using Digitized Data From Sugano, et al. (1993) [1 kg = 2.2 lb; 1 m = 3.28 ft]

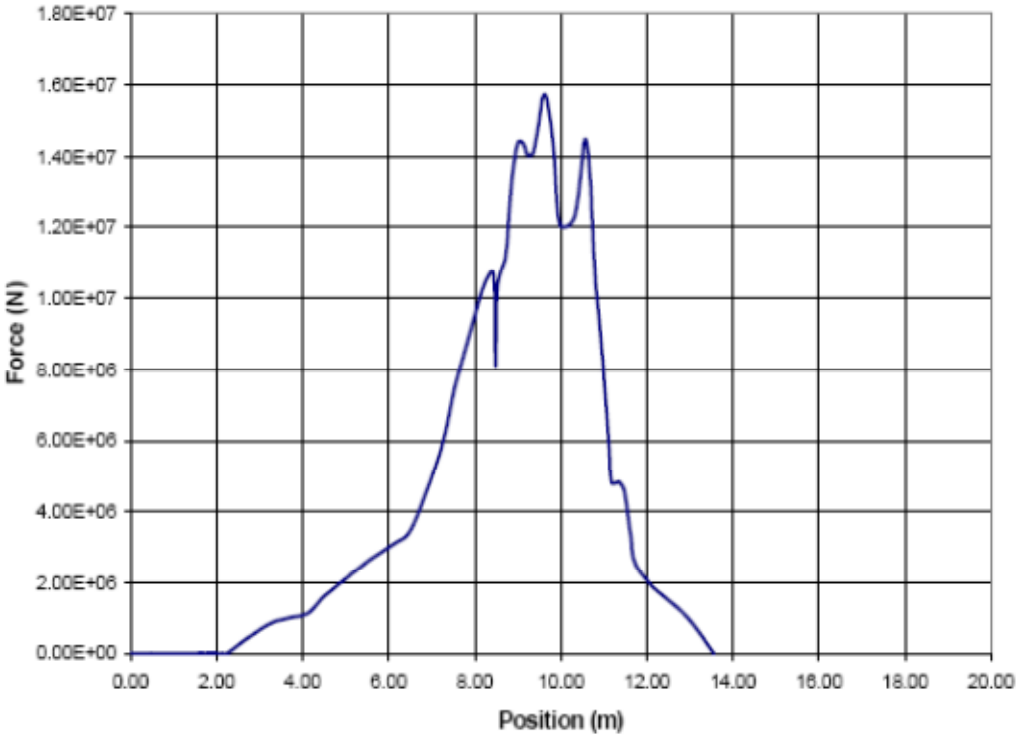

Figure 3-2. Measured Crush Force, P_c, for the F-4 Aircraft Including Skids and Rockets Using Digitized Data (Sugano, et al., 1993) [1 N = 0.225 Lbf; 1 m = 3.28 ft]

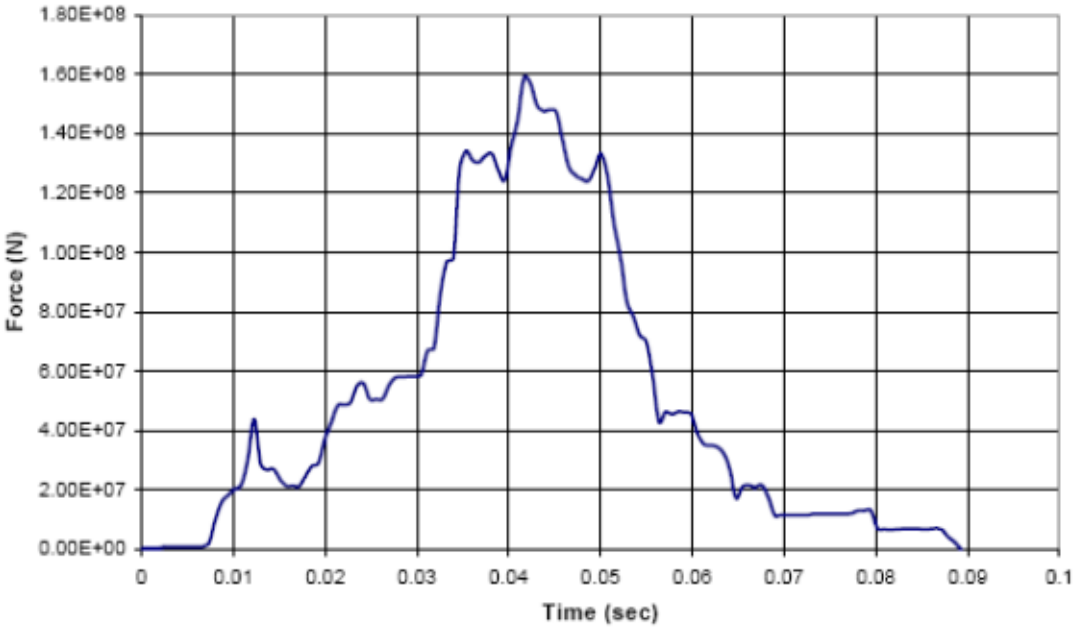

Figure 3-3. Calculated Impact Force on a Rigid Surface Using Riera Method (Riera, 1968) at a Speed of 215 m/s [1 N = 0.225 Lbf]

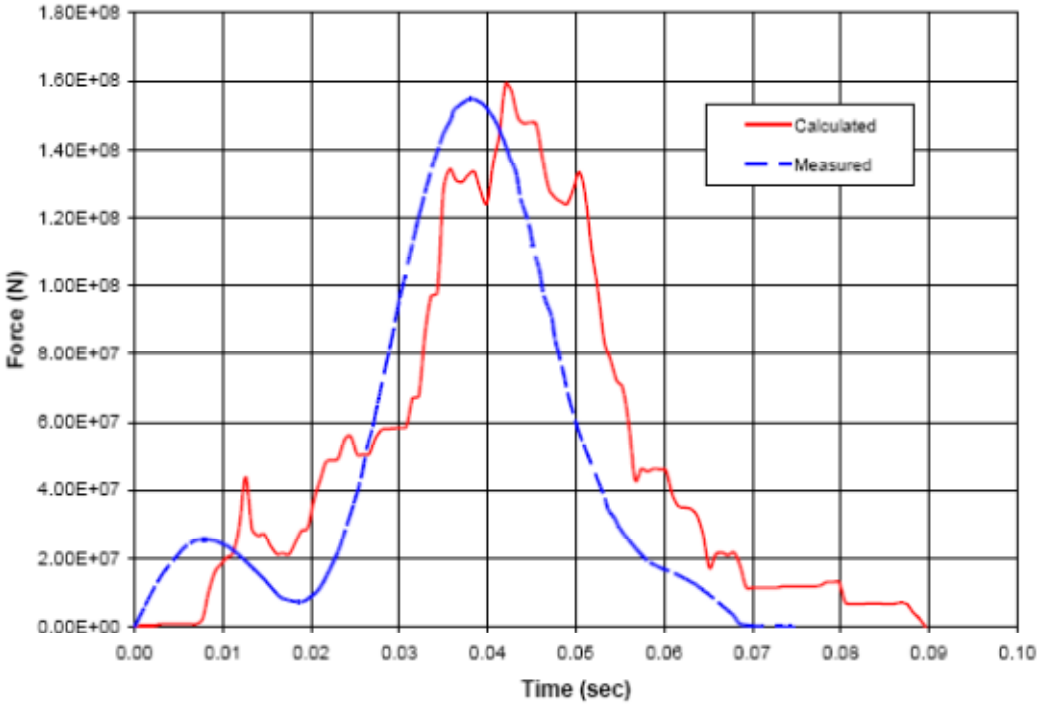

Figure 3-4. Comparison of Measured (Sugano, et al., 1993) and Calculated Impact Forces for the F-4 Aircraft Including Skids and Rockets [1 N = 0.225 Lbf]

Notice that except for a slight time shift, the impact forces are in excellent agreement, with the calculated maximum impact force being only 2.6 percent higher than the maximum measured impact force. The reason for the slight time shift in Figure 3-4 can be determined by examining the experimental data shown in Figures 3-1 and 3-2, as Sugano, et al. (1993) reported. From Figures 3-1 and 3-2, because the mass per unit length and impact forces are essentially zero for a distance of 1.6 m [4.8 ft] from the nose of the aircraft, the calculated impact forces using the Riera method (Riera, 1968) will be essentially zero in this region.

As an additional comparison between the experimental data and the calculations the Riera method (Riera, 1968) produced, the impact forces in Figure 3-4 were integrated to obtain the total impulse delivered to the rigid surface. As shown in Figure 3-5, the total impulse the Riera method calculated is overestimated by 22.2 percent, thus making the Riera method considered conservative.

To improve the correlation between the impulse force calculated using the Riera method (Riera, 1968) and the experimental data, Sugano, et al. (1993) showed that uniformly reducing the aircraft mass per unit length μ by a factor of 0.9 produced the best fit to measured data. However, based on Figure 3-5, the data match very well until approximately 0.05 seconds into the impact event. Therefore, Cox, et al. (2006) suggested that rather than reducing the mass uniformly along the length of the aircraft, a mass adjustment factor that reduces the mass near the tail of the aircraft appears more suitable. The reasoning behind this approach is that, as debris from the crash builds up on the rigid surface, the debris spreads and strikes the rigid surface obliquely, reducing its effect. This effect is greatest near the tail of the aircraft.

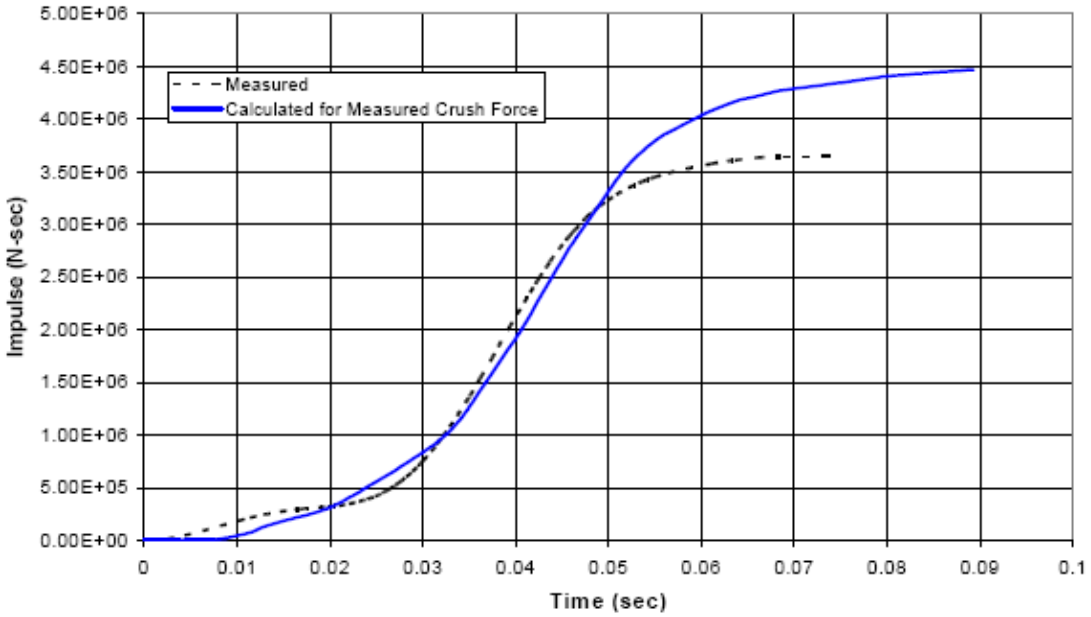

Figure 3-5. Comparison of Measured (Sugano, et al., 1993) and Calculated Impulse for the F-4 Aircraft Including Skids and Rockets [1 N = 0.225 Lbf]

The mass adjustment factor, specific to this case, is shown versus the nondimensional length (x/L) of the aircraft in Figure 3-6. Applying this mass adjustment factor to the calculations

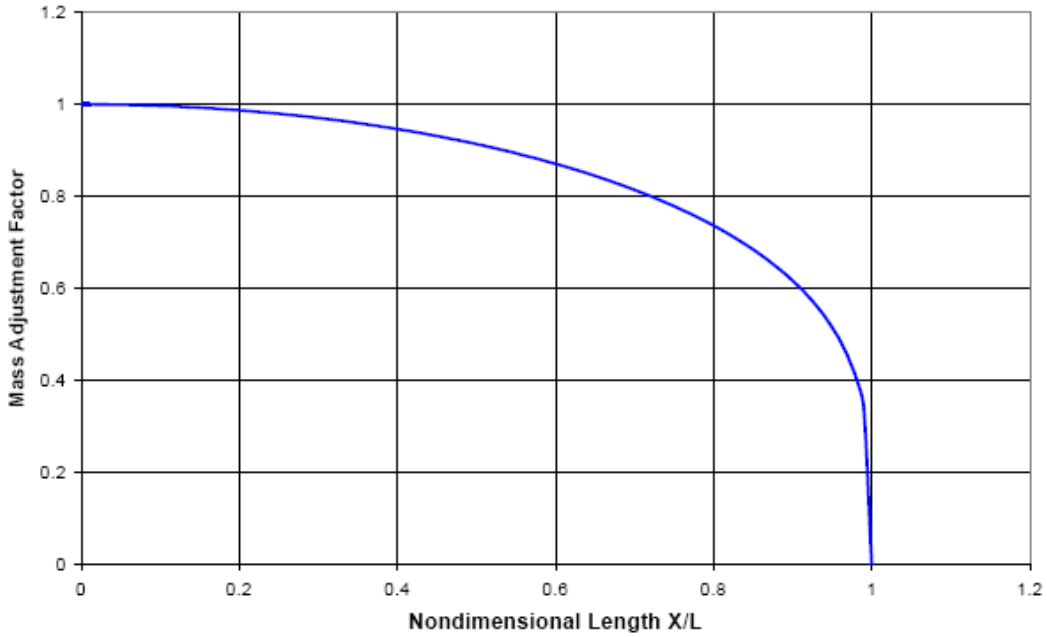

Figure 3-6. Proposed Nonlinear Mass Adjustment Factor Used in Calculation of Impulse Force (Cox, et al., 2005)

using the Riera method (Riera, 1968), the impulse force is reduced to within 10 percent of the measured value as shown in Figure 3-7. Using the same mass adjustment factor on the calculated impact force produces a slightly lower peak in magnitude than the measured impact force as shown in Figure 3-8.

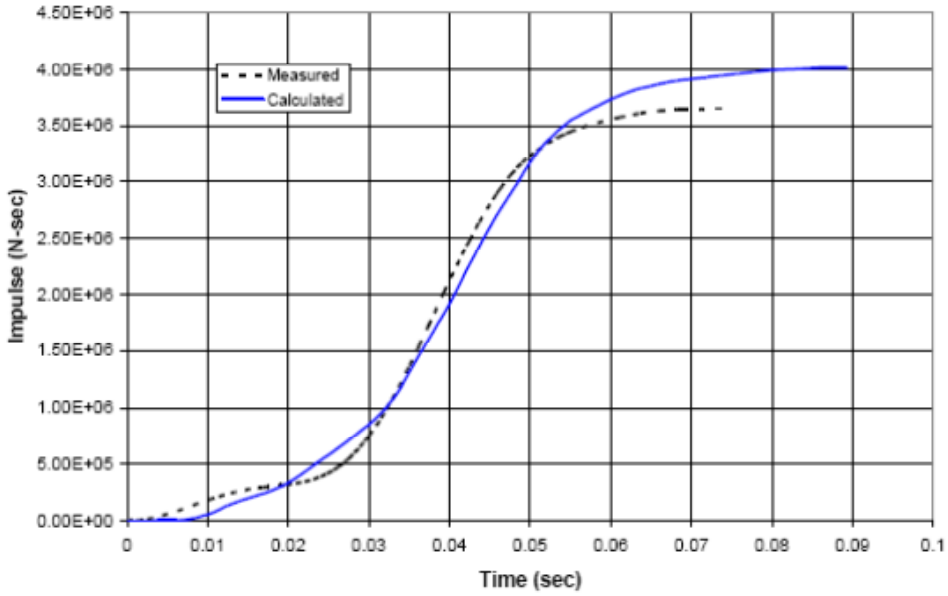

Figure 3-7. Comparison of Calculated Impulse Using Mass Adjustment Factor to Measured Impulse (Sugano, et al., 1993) for the F-4 Aircraft Including Skids and Rockets [1 N = 0.225 Lbf]

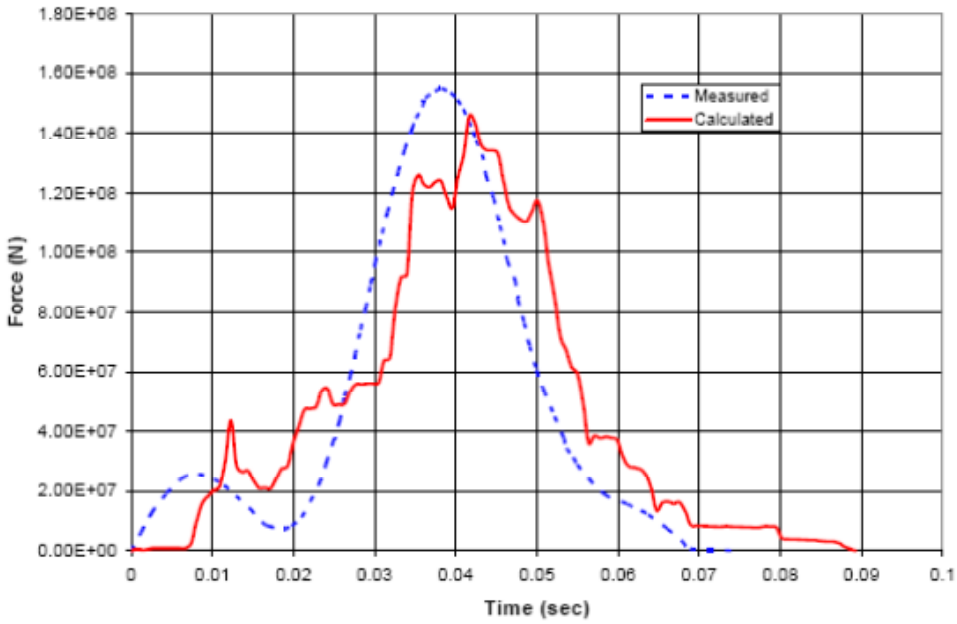

Figure 3-8. Comparison of Calculated Impact Force Using Mass Adjustment Factor to the Measured Force (Sugano, et al., 1993) for the F-4 Aircraft with Skids and Rockets [1 m = 3.28 ft]

3.4 Evaluation of the Full-Scale F-4 Impact Test Target Response

This section evaluates the global response of the large concrete block target used in the full-scale F-4 aircraft impact testing presented in Sugano, et al. (1993). An additional component of the experimental testing in Sugano, et al. (1993) was to evaluate the overall force-time history resulting from the F-4 crashing into the concrete block target (essentially a rigid wall) at a velocity of 215 m/s [705.4 ft/s]. As described in Sugano, et al. (1993), the concrete block rested on a concrete platform that incorporated air bearings to support the weight of the block and platform.

The numerical simulations of the test consisted of creating a finite element model representing the large 7.0 × 7.0 × 3.66-m [22.9 × 22.9 × 12.0-ft] concrete block. Force-time loads taken from the experiment of Sugano, et al. (1993) and calculated force-time loads using the Riera method (Riera, 1968) are applied to the concrete block target. The concrete block's global response is compared to test results of Sugano, et al. (1993).

3.4.1 Finite Element Modeling of the Concrete Block Target

An LS-DYNA finite element model representing the concrete block target was constructed using a mesh of 75,505 solid elements. The solid elements' hourglass control was specified to use the Flanagan-Belytschko viscous form with exact volume integration. The concrete block used the same concrete damage constitutive model described in Chapter 2, and the associated material parameters are those previously listed in Table 2-1.

The finite element concrete block model, having the same dimensions as the block used in the test, had a calculated mass of 468,960 kg [1,033,880 lb] as compared to the actual concrete block's mass of 469,000 kg [1,033,968 lb]. Sugano, et al. (1993) described the concrete block as having reinforcement steel; however, no details were provided. Therefore, no reinforcement steel was included in the finite element concrete block model and the concrete density was adjusted to more closely match the actual mass. Modeling the concrete block without reinforcement steel was deemed adequate for predicting back surface motions because flexure and shear of the block will not occur due to the block thickness {3.66 m [12.01 ft]}. Also, Sugano, et al. (1993) reported that damage to the concrete block produced by the impact of the F-4 aircraft was limited to front face erosion.

Sugano, et al. (1993) stated that air bearings were used to provide for an essentially frictionless contact between the bottom of the platform and the surface that it rested on; however, the air bearings and platform were not modeled in the finite element analysis. Instead, the contact condition between the base of the finite element concrete block and the ground plane was specified to be frictionless to simulate the effect of the air bearings.

The loading of the finite element concrete block model was defined by specifying a force-time history distributed over the impact area. The full-scale test results determined the estimated impact area was 10 m^2 [107.6 ft^2]. For modeling purposes, the shape of the loading area used in the finite element model was idealized as a circle with its center at the center of the block. The force-time history was applied evenly over the circular area to each of the 647 nodes encompassed by the area. The results of the finite element analysis were compared with the available test data of Sugano, et al. (1993), which measured the displacement and velocity at the center of the backside of the concrete block.

3.4.2 Concrete Block Target Response Using Measured and Calculated Load Histories

This subsection contains an evaluation of the concrete block target response that was made by performing two LS-DYNA analyses. The first used the load history obtained directly from the full-scale F-4 impact test, and the second used a load history calculated using the Riera method (Riera, 1968). The load histories were used as input to an LS-DYNA analysis of the concrete block target finite element model. The response was measured in terms of the concrete block's velocity.

The first LS-DYNA analysis used the experimentally measured load obtained directly from the full-scale F-4 impact test that included the sled and the rockets, which were used to accelerate the aircraft. The force-time history used in this analysis is that shown in Figure 3-8 labeled as the "measured" data.

The concrete block velocity-time history predicted by the LS-DYNA analysis and that of the measured test data is shown in Figure 3-9. Good agreement in the maximum velocity is observed between the measured data from the F-4 test and the LS-DYNA results. Figure 3-10 shows a comparison of the displacements, measured on the back face of the concrete block target, for the test data and the LS-DYNA results. In terms of the actual damage to the concrete block from the test, Sugano, et al. (1993) observed a maximum penetration depth of 60 mm [2.36 in] on the front face of the block—partly a result of the engines impacting the block. The penetration depth due to the fuselage was a maximum of 20 mm [0.79 in]. Thus, Sugano, et al. (1993) considered the damage caused by the fuselage insignificant as compared to the damage caused by the engines. The overall damage to the concrete block was characterized as superficial scarring over the impact region (Sugano, et al., 1993). The most significant amount of damage, in the form of concrete spalling, was due to the impact of the carriage sled and rockets (Sugano, et al., 1993).

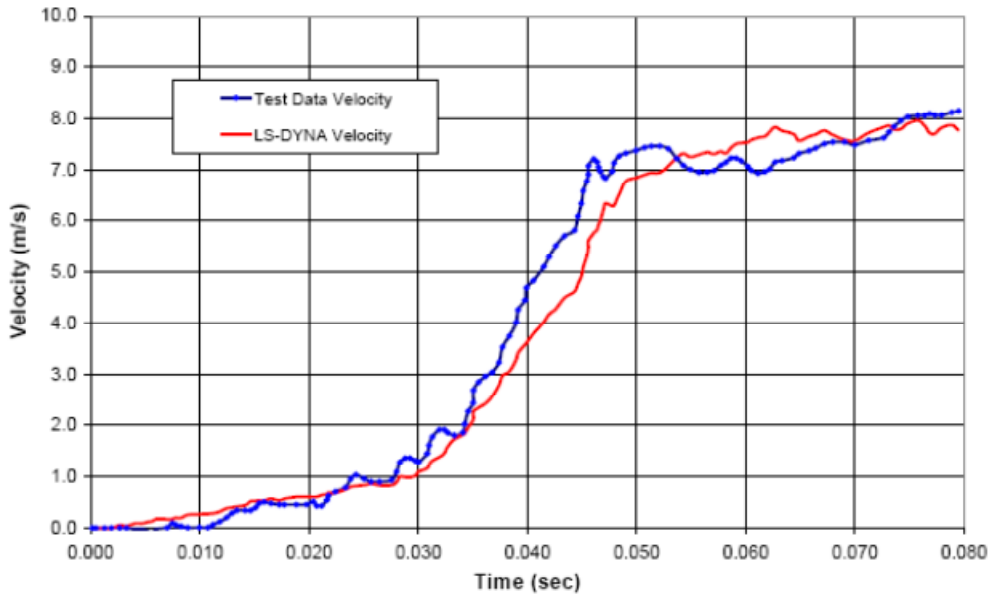

Figure 3-9. Comparison of LS-DYNA Calculated Target Block Velocity to Test Data Target Block Velocity (Using the Measured Load in Figure 3-8) of Sugano, et al. (1993) [1 m = 3.28 ft]

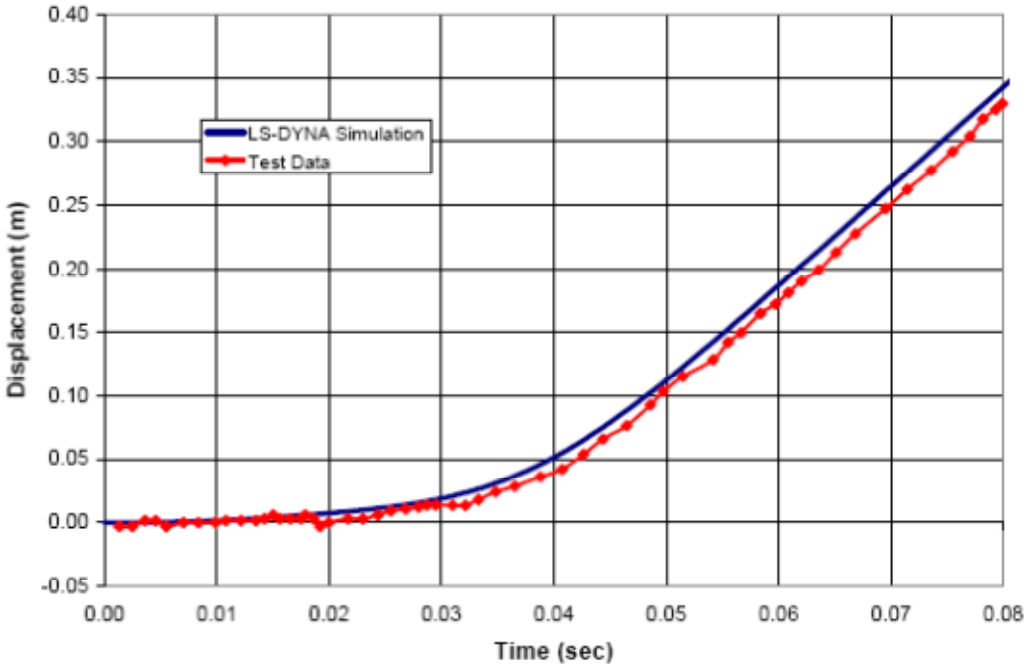

Figure 3-10. Comparison of LS-DYNA Calculated Displacement (Back Face of Target) Time History to Measured Test Data of Sugano, et al. (1993) [1 m = 3.28 ft]

The LS-DYNA results did not show any penetration into the target. This was most likely due to the load being uniformly applied over an idealized circular area. In addition, the finite element mesh used was considered to be relatively coarse. A finer mesh was not used, because the object of the analysis was not to capture the details of the penetration into the block, but rather to determine the overall global response of an essentially rigid structure. Also, because aircraft and sled loads were lumped together and applied over the same circular area, no local penetrations could be captured.

The second LS-DYNA analysis used the input load history calculated using the Riera method (Riera, 1968) to represent the F-4, the carriage sled, and rockets. The calculated load history using the Riera method, shown in Figure 3-11, was applied uniformly over a circular area of the concrete block finite element model.

A comparison of the velocity-time history from the LS-DYNA analysis versus the test data is shown in Figure 3-12. The LS-DYNA results show good overall agreement; however, the final velocity from LS-DYNA using the Riera method is approximately 7 percent higher than the test data velocity. These results tend to confirm the findings in Section 3.2 that the Riera method (Riera, 1968) predicts loads that are conservative.

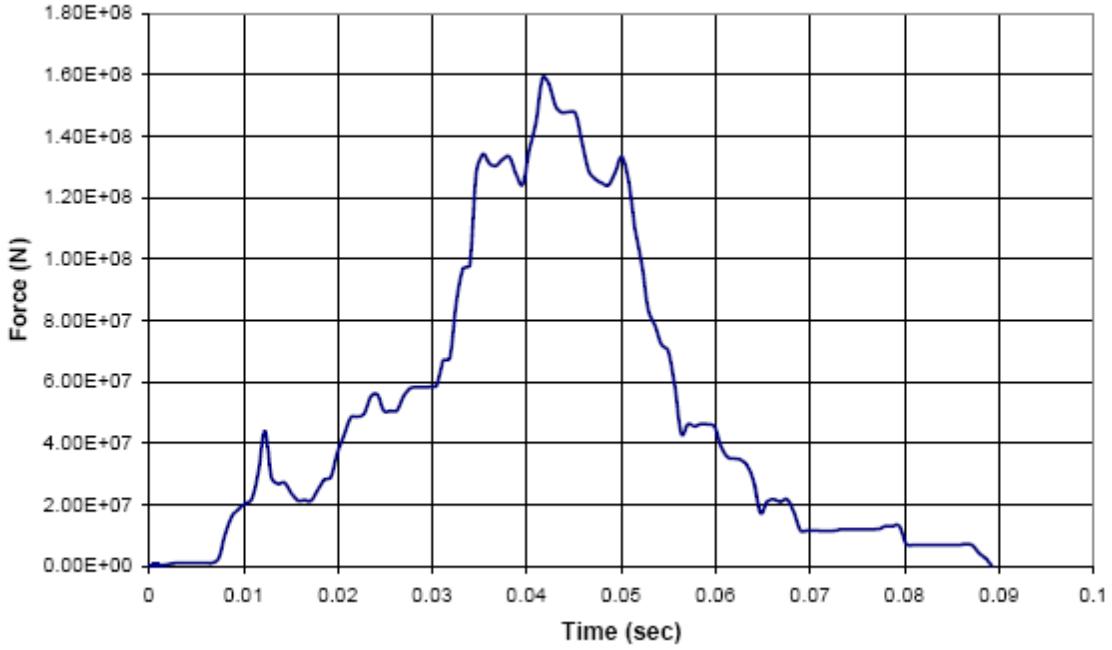

Figure 3-11. Calculated Load-Time History of the Full-Scale F-4 Aircraft Test Using the Riera Method (Riera, 1968) [1 N = 0.225 Lbf]

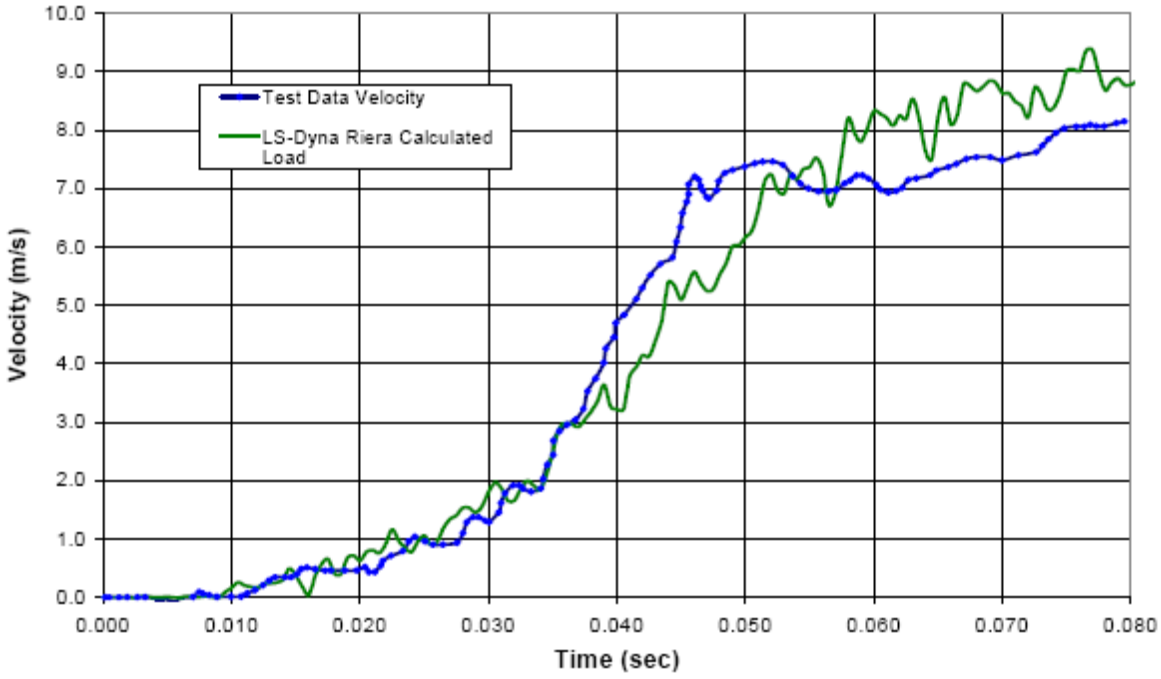

Figure 3-12. Comparison of Test Data (Sugano, et al., 1993) With Simulation Results Using the Riera Calculated Loading [1 m = 3.28 ft]

4 NUMERICAL MODELING OF THE F-15E AIRCRAFT

4.1 Introduction

In Chapter 3, the Riera method (Riera, 1968) (force-time history analysis) was used to calculate the impact force. The Riera method was evaluated to access its accuracy for calculating the impact force as compared to measured data from a full-scale F-4 impact test. The conclusion made in Chapter 3 was that the Riera method is considered conservative.

Another method to evaluate global damage is the missile target interaction analysis method (Hossain, et al., 1997). This method has an advantage over the force-time history analysis method because it can more realistically represent the impact behavior of the aircraft and the target response. A missile target interaction analysis is typically performed using three-dimensional finite element analysis. The finite element method can accurately model the material and geometric nonlinearity of the aircraft and the target unlike the Riera method (Riera, 1968), which is based on the assumption of a rigid target.

In conventional finite element models, elements are directly connected to each other via nodes forming a mesh. The finite element method can have difficulties solving very large deformation problems where significant mesh (element) distortion occurs. Robust element formulation to account for large strains and large rotations in addition to adaptive mesh refinement are typical solutions to handle large deformations. An alternative to conventional finite elements is the mesh-free approach. One such mesh-free approach is known as the smoothed particle hydrodynamics (SPH) method. Because the particles are not directly connected, an SPH mesh can undergo very large deformations while maintaining stability. Therefore, the SPH method is an effective alternative to the conventional finite element approach when performing an analysis in which large deformations leading to complete destruction are expected and the primary mode of loading is due to mass/momentum.

LS-DYNA has the capability to construct SPH models. The LS-DYNA Theory Manual (Livermore Software Technology Corporation, 2003b) provides theoretical details of the SPH method and how it is implemented in LS-DYNA. The LS-DYNA Theory Manual provides guidance on coupling conventional finite element models with SPH models through the use of contact conditions. It also notes that proper SPH meshes should be as uniform as possible (Livermore Software Technology Corporation, 2003b).

The following sections detail developing an SPH model for simulating aircraft crash impact into a reinforced concrete structure.

4.2 A Smoothed Particle Hydrodynamics Model of the F-15E

This section details constructing the F-15E aircraft model using the SPH method. Initially, a surface mesh of an F-15 was constructed using TrueGrid (XYZ Scientific Applications, Inc., 2006). The external geometry of the aircraft was imported into TrueGrid from a computer-aided design (CAD) surface file, in initial graphics exchange specification (IGES) format, of the F-15 aircraft. Images of the surface mesh for the F-15, created from the IGES file, are shown in Figure 4-1. Additional details of the initial F-15 model are given Cox, et al. (2007). The F-15E model used in this report has a more refined and evenly spaced mesh.

Figure 4-1. Finite Element Surface Model of the F-15 Aircraft

After the initial surface mesh was created, it was converted into SPH particles using the LS-DYNA preprocessing software LS-PrePost (Livermore Software Technology Corporation, 2003c). The geometry file for the F-15E provided no details on the internal structural components (e.g., stringers, frames, bulkheads), as it only represented the external skin of the aircraft. Therefore, it was necessary to include the mass of the internal structures in the aircraft's external skin. Table 4-1 lists the major aircraft components and their weights.

Table 4-1. F-15E Weights*

Components	Weights
Structure	**8,936 kg [19,700 lb]**
Fuselage	4,672 kg [10,300 lb]
Landing Gear	1,179 kg [2,600 lb]
Tail	499 ka [1,100 lb]
Wing	2,585 kg [5,700 lb]
Power Plant	**4,354 kg [9,600 lb]**
Engines	3,357 kg [7,400 lb]
Nacelles	998 kg [2,200 lb]
Equipment	**1,225 kg [2,700 lb]**
Fixed	771 kg [1,700 lb]
Mission	454 kg [1,000 lb]
Useful Load	**19,232 kg [42,400 lb]**
Fuel	15,604 kg [34,400 lb]
Payload	3,629 kg [8,000 lb]
Takeoff Weight	**33,747 kg [74,400 lb]**

*Hossain, Q.A., R.P. Kennedy, R.C. Murray, K. Mutreja, and B.P. Tripathi. "Structures, Systems, and Components Evaluation Technical Support Document. DOE Standard, Accident Analysis for Aircraft Crash into Hazardous Facilities." UCRL–ID–123577. Livermore, California: Lawrence Livermore National Laboratory, United States Department of Energy. 1997.

Because mass distribution data were not available for the F-15E, various available resources were used to make assumptions on the location of major components.

NRC furnished an isometric drawing of the F-15, which provided visual information on the location of various internal components; however, the drawing was not dimensioned. The isometric drawing and overall aircraft dimensions from the external surface file were used to estimate the location of internal and external fuel tanks, landing gear, equipment, payload, and engines for the aircraft.

To represent the aircraft's internal structure, a known mass distribution of the F-4 Phantom fuselage (Sugano, et al., 1993) was scaled to the length of the F-15. This distribution was then used as the fuselage mass distribution for the F-15E.

The fuselage mass plus the mass of other components (landing gear, tail, wing, equipment, and payload) were all placed in the external skin of the aircraft. The mass contributions from each component were added at their respective positions along the length of the aircraft. Figure 4-2 shows a plan view of the aircraft skin mesh, divided into 1-m [3.3-ft] segments along its length. The locations of the aircraft component weights are also shown. The component labels shown in Figure 4-2, except for the fuselage, have their total weights (from Table 4-1) distributed evenly across the number of segments shown.

Each colored segment contains a collection of SPH particles. The particles in a given segment all have the same mass. The mass of each particle is therefore based on the total mass of the segment divided by the number of particles in the segment. In LS-DYNA, the user explicitly

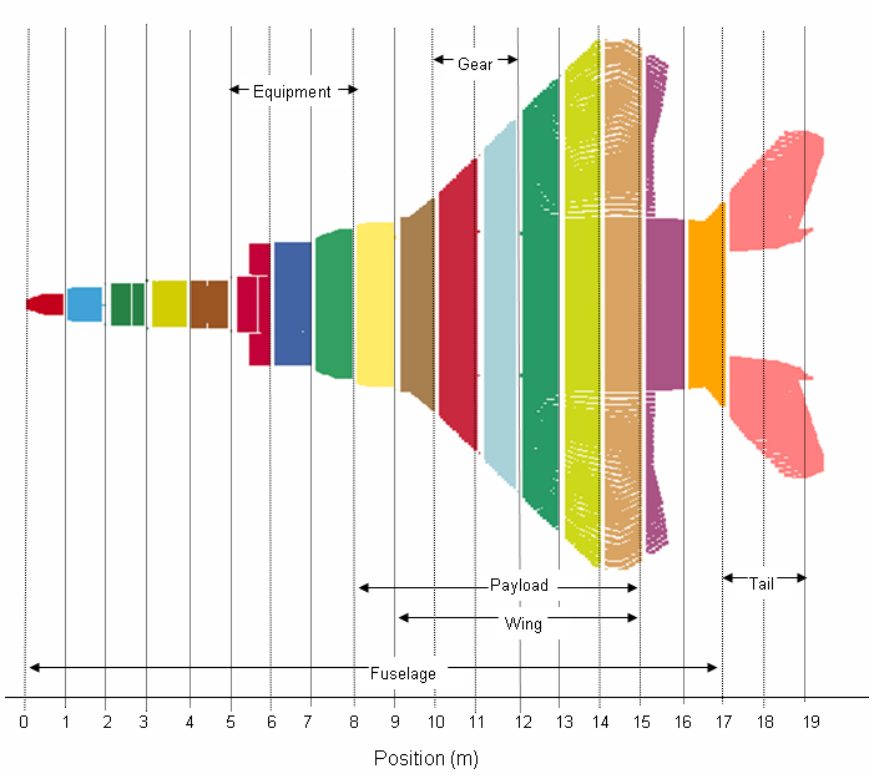

Figure 4-2. Grouping of SPH Particles in 1-m [3.3-ft] Increments Along the F-15E With Positions Indicated for Various Parts of the Aircraft

defines the particle masses. To automate this process, a program was written in FORTRAN, which steps along the length of the model at predefined spatial increments and assigns the appropriate mass to each particle contained within a segment.

The aircraft fuel was modeled separately from the skin. Three major fuel loads were considered: internal fuel, external tanks, and the conformal fuel tanks. Fuel distribution for the F-15E was obtained from Aerospaceweb.org (2011), which indicated an internal fuel capacity (fuselage and wings) of 5,953 kg [13,125 lb] and an external capacity of 9,818 kg [21,645 lb]. Thus, the total fuel load is slightly higher than that given in Table 4-1. External capacity was approximately equal for each of the three external tanks and the two conformal fuel tanks. Location of the external tanks was determined from the CAD model. The location of the internal fuel was estimated by scaling its position from the isometric drawing. All fuel was meshed with SPH particles.

The engines and nacelles also were modeled separately from the fuselage. The F100-PW-229 engine and nacelle weights are given in Table 4-1. The overall length and diameter of the engines were obtained from Pratt and Whitney (2011) and by scaling the isometric drawing. Based on the isometric drawing, the total engine package has two components: the engine (consisting of shafts, compressor, turbine, and combustor) and the nacelles (consisting of the afterburner section, nozzles, and general engine containment). The main engine component has a length of 3 m [118 in], and the nacelle section aft of the engines has a length of 2.3 m [90 in]. The average diameter of the engine is 1 m [40 in]. Therefore, each engine model consisted of a forward section, with a total weight of 1,678 kg [3,700 lb] evenly distributed along the length, and an aft section, with a total weight of 544 kg [1,200 lb] evenly distributed along its length. The engines were also meshed with SPH particles.

The entire aircraft mesh including all internals is shown in Figure 4-3. Also shown is the aircraft with the skin removed, exposing the fuel and engine components. The model has a total of 135,049 SPH particles.

The model represented a total weight of 33,472 kg [73,793 lb]. The actual weight breakdown is shown in Table 4-2. The total weight is just under the takeoff weight provided in Table 4-1 due to roundoff when calculating the fuselage weight.

After construction of the SPH model, its mass distribution was evaluated to ensure it reasonably represented the true mass distribution of the F-15E, which was not known other than the details provided in Table 4-1. The initial mass distribution calculations were performed in Excel at 1-m [3.3-ft] increments because the model is based on all SPH particles having equal mass within each 1-m [3.3-ft] segment along the aircraft. Three calculations were performed: (i) mass distribution of the fuselage including all added components in Figure 4-4, (ii) mass distribution of the fuel in Figure 4-5, and (iii) mass distribution of the entire aircraft including components, fuel, and engines in Figure 4-6.

4.3 Materials and Parameters

The skin of the aircraft was modeled using aluminum as the material. The engines were modeled using steel. Both the aluminum and steel were modeled with the LS-DYNA

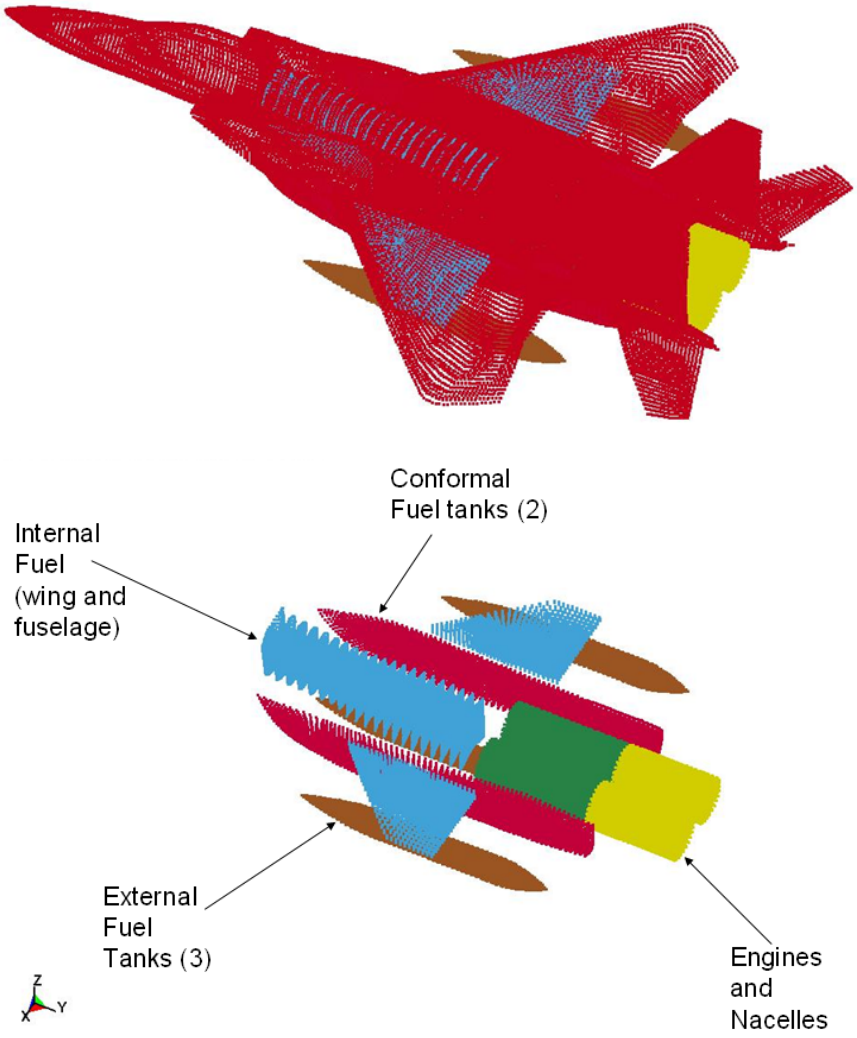

Figure 4-3. Full SPH Model of the F-15E (Top) and SPH Model With Aircraft Skin Removed (Bottom)

Table 4-2. Mass of F-15E Components in the SPH Model	
Component	**Mass**
Engines	4,326 kg [9,537 lb]
Fuel	15,773 kg [34,774 lb]
Internal	5,954 kg [13,126 lb]
External	5,356 kg [11,808 lb]
CFT	4,465 kg [9,844 lb]
Fuselage (Includes All Major Components)	13,371 kg [29,477 lb]
Total	33,472 kg [73,793 lb]

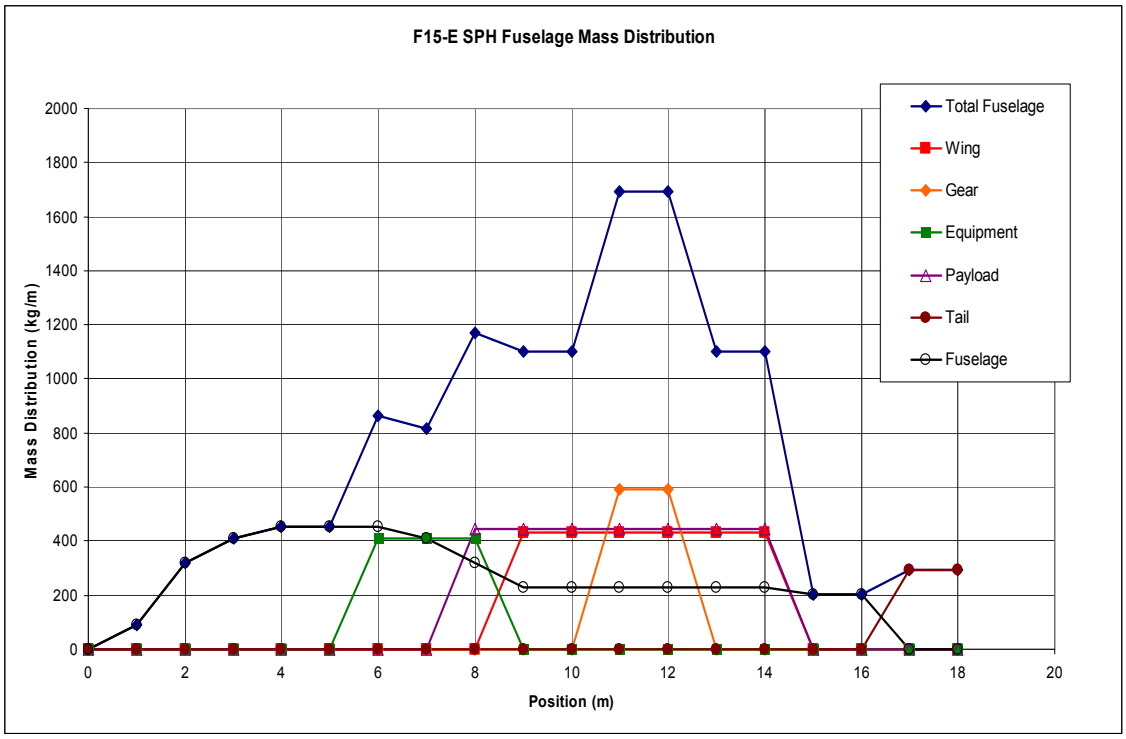

Figure 4-4. Fuselage and Component Mass Distribution as Compiled in 1-m [3.3-ft] Increments From the SPH Model

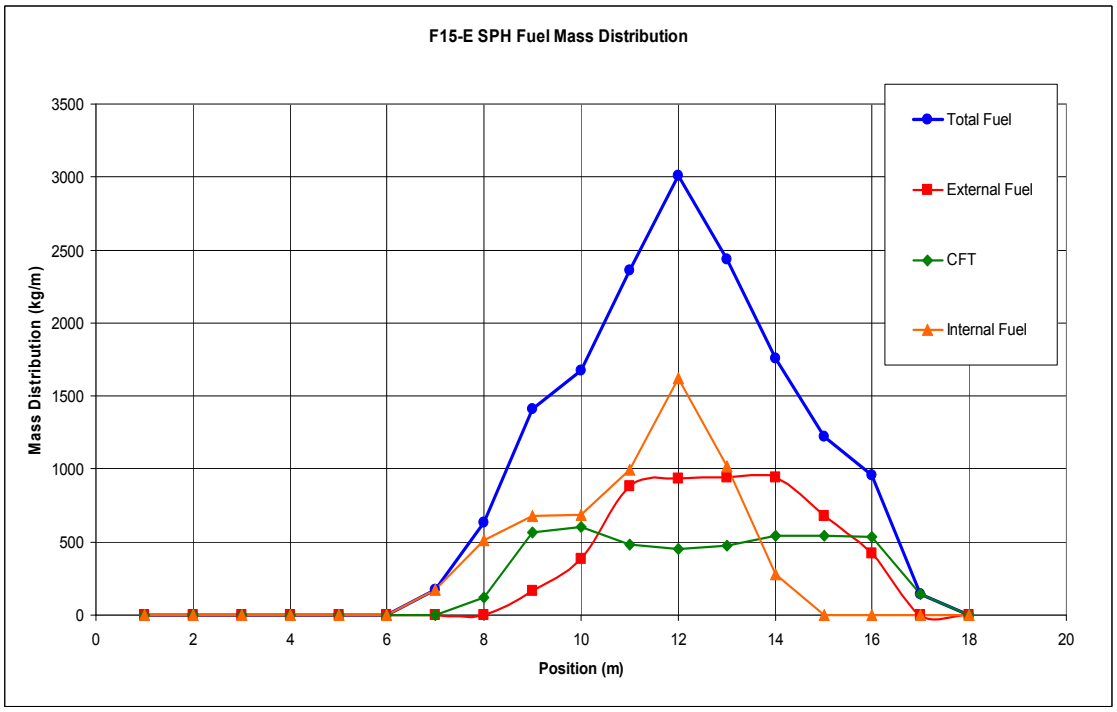

Figure 4-5. Fuel Mass Distribution as Compiled in 1-m [3.3-ft] Increments From the SPH Model

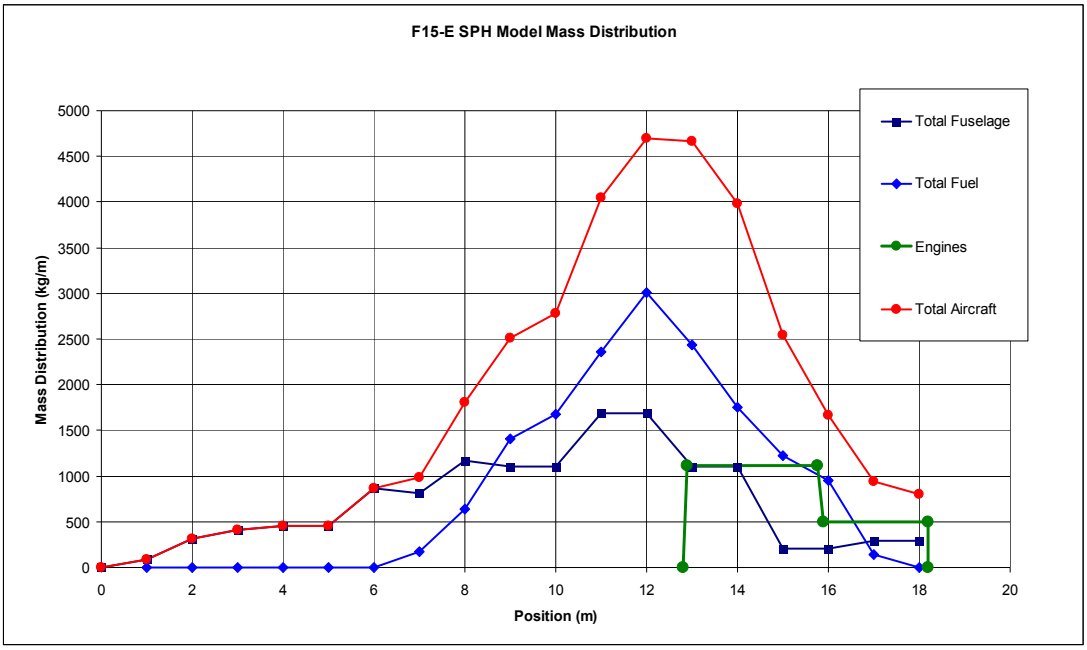

Figure 4-6. Total Aircraft Mass Distribution as Compiled in 1-m [3.3-ft] Increments From the SPH Model

*MAT_PLASTIC_KINEMATIC material model (Livermore Software Technology Corporation, 2003a). Table 4-3 lists the values used in the initial analysis.

The fuel was modeled as a liquid using the LS-DYNA keyword *MAT_NULL, which defines a material with no yield strength and behaves with fluidlike characteristics. The use of *MAT_NULL requires an equation of state that determines the hydrostatic, or bulk, behavior of the material. The LS-DYNA keyword *EOS_GRUNEISEN is used to define the equation of state (Livermore Software Technology Corporation, 2003a). Table 4-4 lists the fluid parameters used in LS-DYNA. Note that the density of the fuel has been adjusted to that of aluminum. This was required for computational stability. LS-DYNA, and the SPH method in general, does not handle situations where vastly different densities (or masses) are found between closely neighboring particles. It is important to note that this does not affect the weight of the fuel, as the mass is explicitly defined at each node.

Table 4-3. Metal Material Properties Used in the SPH Model

	Aluminum	Steel
Density	2,770 kg/m^3 [173 lb/ft^3]	7,830 kg/m^3 [489 lb/ft^3]
Young's Modulus	69.0 × 10^9 Pa [10,008 ksi]	2.01 × 10^{11} Pa [29,152 ksi]
Yield Stress	95.0 × 10^6 Pa [13.8 ksi]	3.49 × 10^7 Pa [5.06 ksi]
Poisson Ratio	.33	.3
Failure Strain	0.4	0.05

Table 4-4. Properties for Fluids Used in the SPH Model

*MAT_NULL	
Density	2,770 kg/m^3 [173 lb/ft^3]
Pressure Cutoff	−1.0 Pa [−1.45 × 10^{-7} ksi]
Dynamic Viscosity	100 Pa-s [1.45 × 10^{-5} ksi-s]
Gruneisen Constants	
C	1,560 m/s [1,560 ft/s]
S1	2.0
Gamma	1.1

5 RIGID WALL IMPACT ANALYSIS

5.1 Introduction

As discussed in Section 3.1, the Riera method (Riera, 1968) makes the assumption that the target is rigid. Thus, in this chapter, impact forces based on a rigid wall were calculated. The impact forces were calculated by two methods: the Riera method (Riera, 1968) and using the smooth particle hydrodynamic (SPH) aircraft model described in Chapter 4. Impact forces computed by the Riera method are presented in Section 5.2, and Section 5.3 presents the impact forces using the SPH aircraft model.

5.2 Impact Forces Using the Riera Method

As was discussed in Chapter 3, the Riera method (Riera, 1968) requires that the mass distribution and the crush force along the aircraft's length are known. Because the F-15E mass distribution was not available for this project, values from the SPH model (Figure 4-6) described in Chapter 4 were used. To obtain a crush force, values Sugano, et al. (1993) reported for the F-4 aircraft (Figure 5-1) were scaled to obtain the F-15E values. This approach is believed to be suitable because the F-15E is similar in size and weight to the F-4 aircraft as shown in Table 5-1.

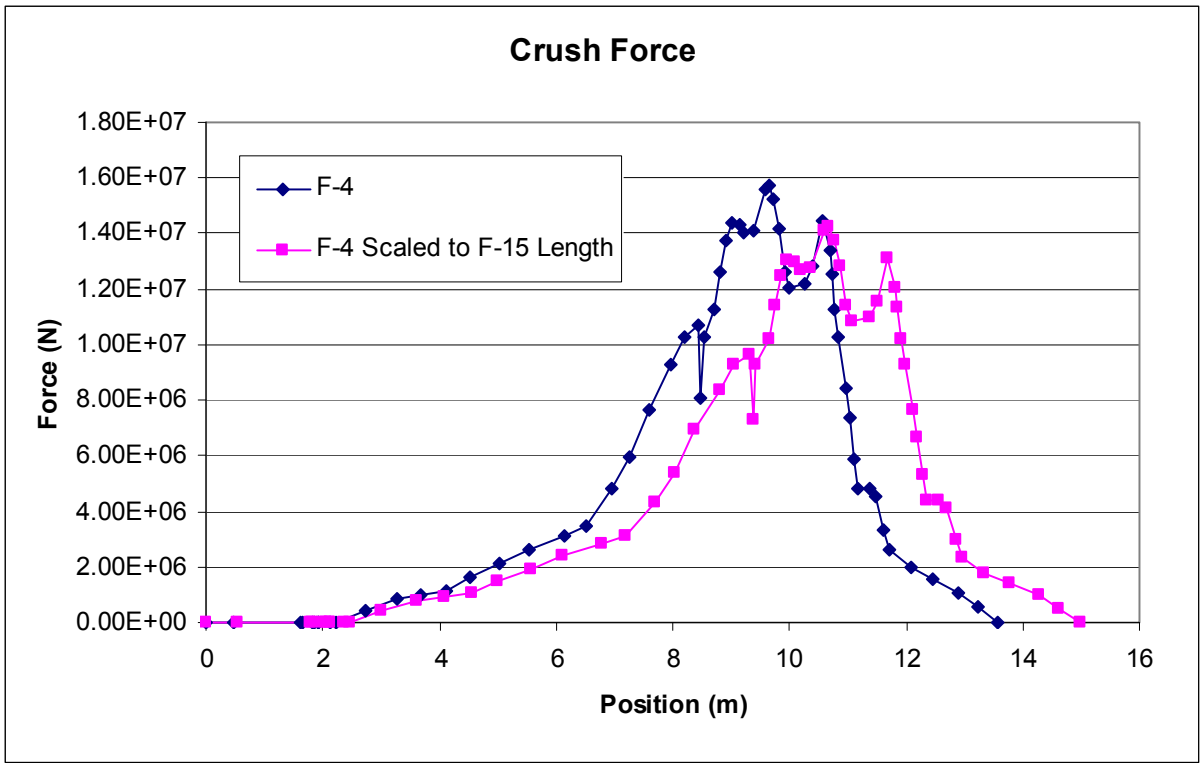

Figure 5-1. Crush Force for the F-4 (Sugano, et al., 1993) and Crush Force for the F-4 Scaled to the Length of the F-15E [1 m = 3.28 ft; 1 N = 0.22 lbf]

Table 5-1. Data for the F-4 and F-15E Aircraft		
Aircraft Component	**F-4**	**F-15E**
Overall Length	17.8 m [58.4 ft]	19.43 m [63.75 ft]
Wing Span	11.8 m [38.7 ft]	13.05 m [42.82 ft]
Weight Empty	12,776 kg [28,171 lb]	14,376 kg [31,700 lb]
Maximum Ordinance Load	8,480 kg [18,698 lb]	11,111 kg [24,500 lb]
Maximum Takeoff Weight	27,900 kg [61,519 lb]	33,560 kg [74,000 lb]
Internal Fuel	4,735 kg [10,440 lb]	5,953 kg [13,126 lb]
Number of Engines	2	2
Engine Type	GE J79	F100-PW-229
Engine Weight, Each	1,791 kg [3,949 lb]	1,678 kg [3,700 lb]

Scaling was performed in two steps: (i) data for the F-4 were scaled by length to obtain the modified values for the F-4 also given in Figure 5-1 and (ii) the values were scaled linearly by the unit masses of the two aircraft (higher unit mass produced higher crush force) to obtain the F-15E values in Figure 5-2. When scaling by length, the total area under the curve (force times distance) was unchanged. When scaling by the unit mass, the crush force for the F-15E was found to be higher than for the F-4 because its unit mass was higher than that of the F-4 at some locations along the length of the aircraft.

The Excel spreadsheet program, previously described in Section 3.3, calculated the impact forces using the Riera method for the F-15E aircraft impacting a rigid surface at 112 m/s [367 ft/s] (Figure 5-3). These calculations used adjustment factors for mass and crush force that were previously shown in Section 3.3 (Figure 3-7) to provide good correlation to measured

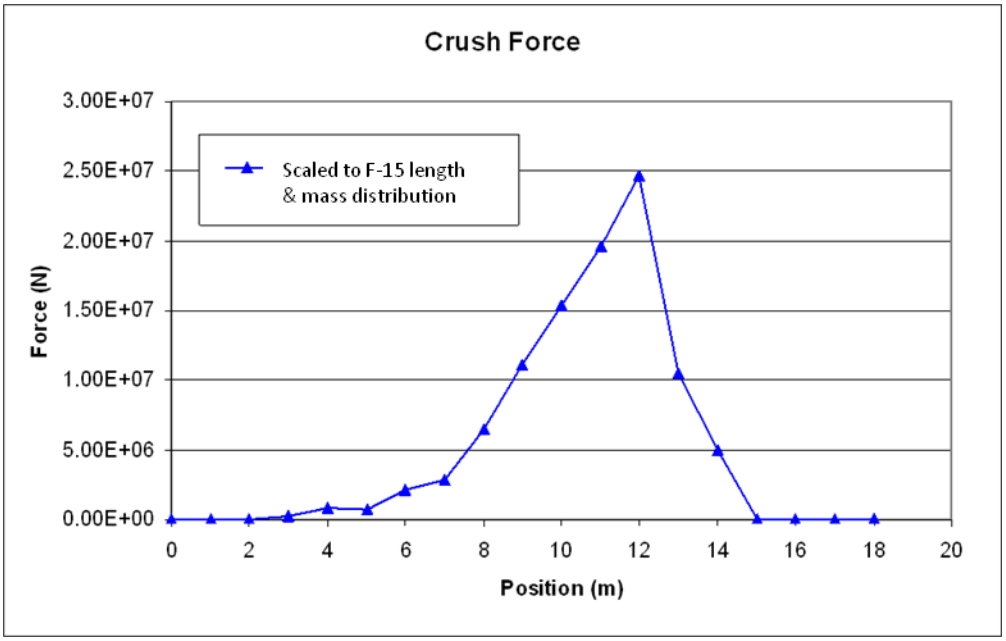

Figure 5-2. Crush Force for the F-15E Scaled from the F-4 Aircraft Using Distributed Mass in Figure 4-6 {190 m/s [623 ft/s]; 1 N = 0.22 lbf}

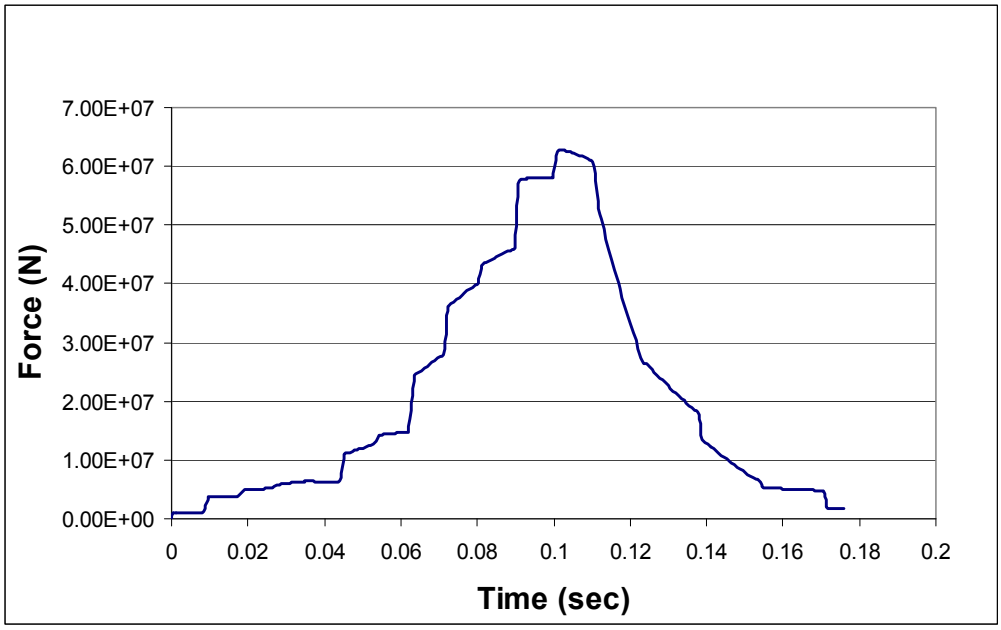

Figure 5-3. Impact Force Computed by the Riera Method (Riera, 1968) for the F-15E Impacting a Rigid Surface at 112 m/s [367 ft/s]. Riera Calculations Used the Mass Distribution from Figure 4-6 and Crush Force from Figure 5-2 {1 N = [0.22 lbf]}.

impulse force for the F-4 aircraft. A constant adjustment factor (constant over the full length of the aircraft) of 0.75 was applied to the crush force, and the nonuniform adjustment factor (Figure 3-7) was used for the distributed mass.

Similar calculations at different impact velocities yielded the impact forces in Figures 5-4 and 5-5. Subsequently, revisions were made to the mass distribution of the F-15E by summing particle masses from the SPH model over different increments along the length of the aircraft. Smaller increments produce more variation in the unit mass along the aircraft's length. However, if the increments are too small, no SPH particles may lie in the interval and a zero mass value is obtained. Such values are artificial and are avoided by increasing the interval over which the particle masses are summed. Therefore, an increment of 0.4 m [1.3 ft] was used in the final calculations.

5.3 Impact Forces Using the SPH Model

LS-DYNA analyses were performed using the SPH aircraft model discussed in Chapter 4 to simulate an F-15E impacting a rigid wall. The simulations used the LS-DYNA RIGID_WALL_FORCES option (Livermore Software Technology Corporation, 2003a), which places a rigid wall at a defined location and calculates the equivalent reaction force on the wall due to the aircraft impact. The simulations were performed for aircraft speeds of 112 and 190 m/s [367 and 623 ft/s]. Figures 5-6 and 5-7 show the results of the SPH model simulation along with a comparison to the Riera-calculated impact forces, previously shown in Figures 5-3 and 5-4.

Figure 5-7 indicates that the SPH model shows better agreement with the Riera calculation at the higher impact speed of 190 m/s [623 ft/s]. However, Figure 5-6 shows that at the lower

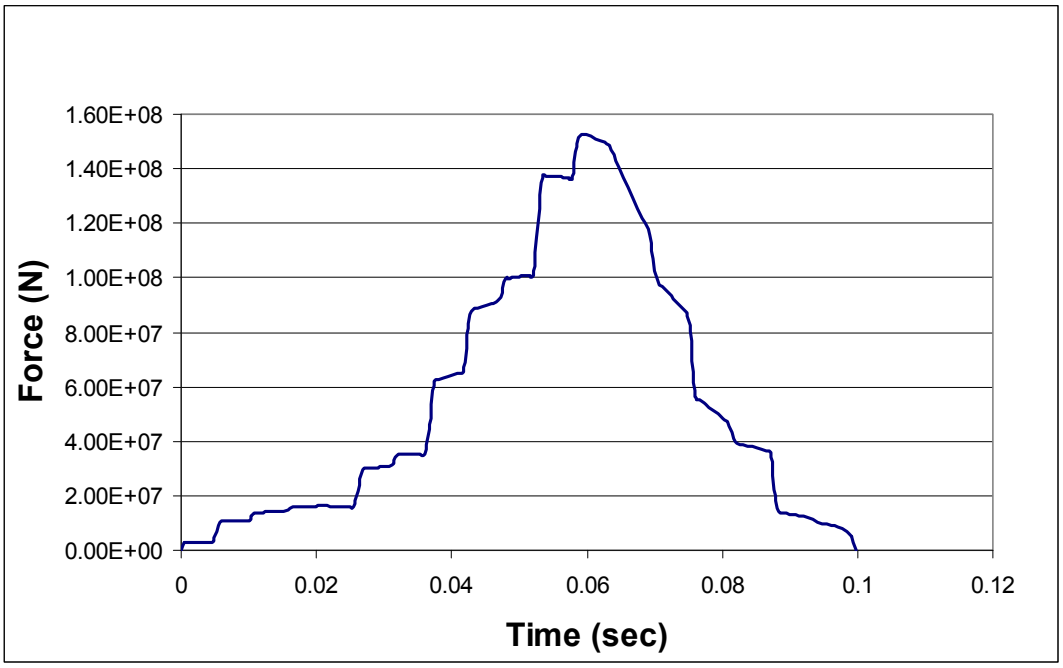

Figure 5-4. Impact Force Computed by the Riera Method (Riera, 1968) for the F-15E Impacting a Rigid Surface at 190 m/s [623 ft/s]. Riera Calculations Used the Mass Distribution from Figure 4-6 and Crush Force from Figure 5-2 {1 N = [0.22 lbf]}.

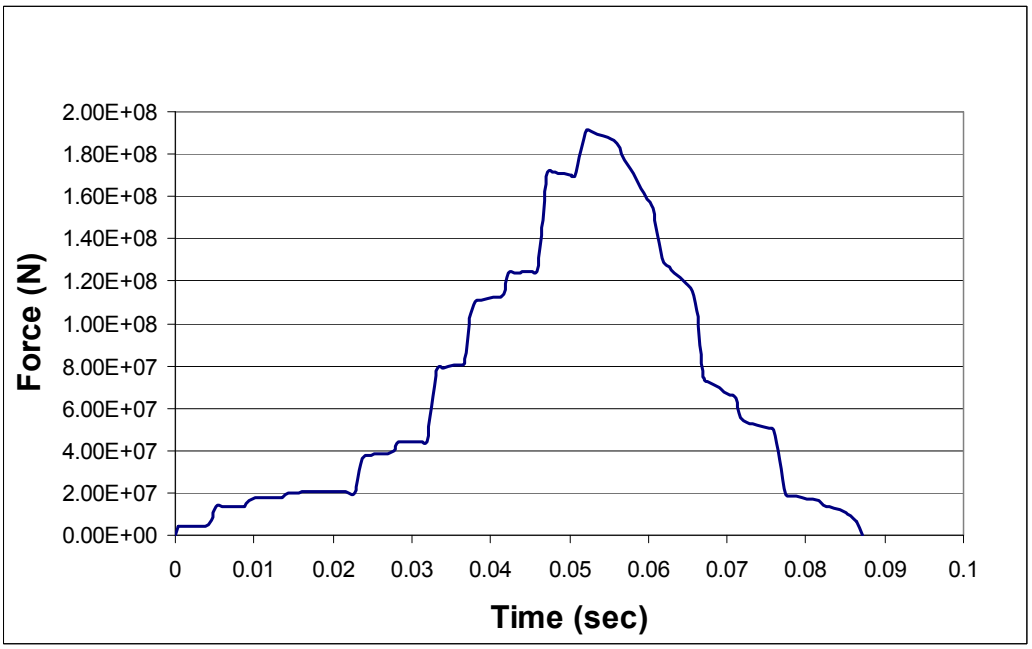

Figure 5-5. Impact Force Computed by the Riera Method (Riera, 1968) for the F-15E Impacting a Rigid Surface at 215 m/s [705 ft/s]. Riera Calculations Used the Mass Distribution from Figure 4-6 and Crush Force from Figure 5-2 {1 N = [0.22 lbf]}.

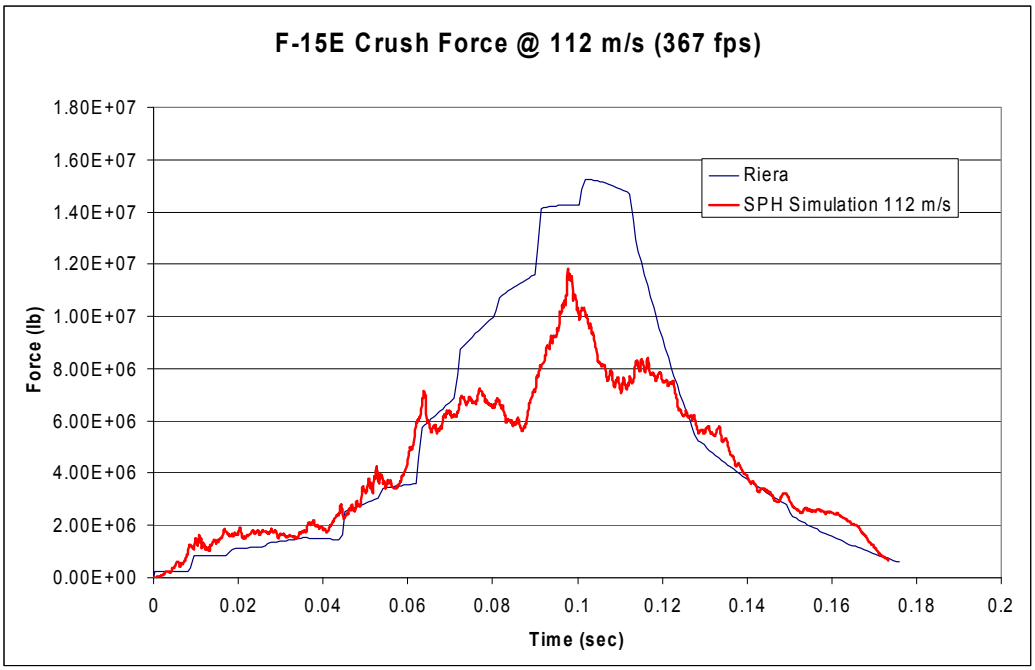

Figure 5-6. Comparison of Impact Forces Calculated by the Riera Method (Riera, 1968) and the SPH Model for an Impact Velocity of 112 m/s [367 ft/s] into a Rigid Surface

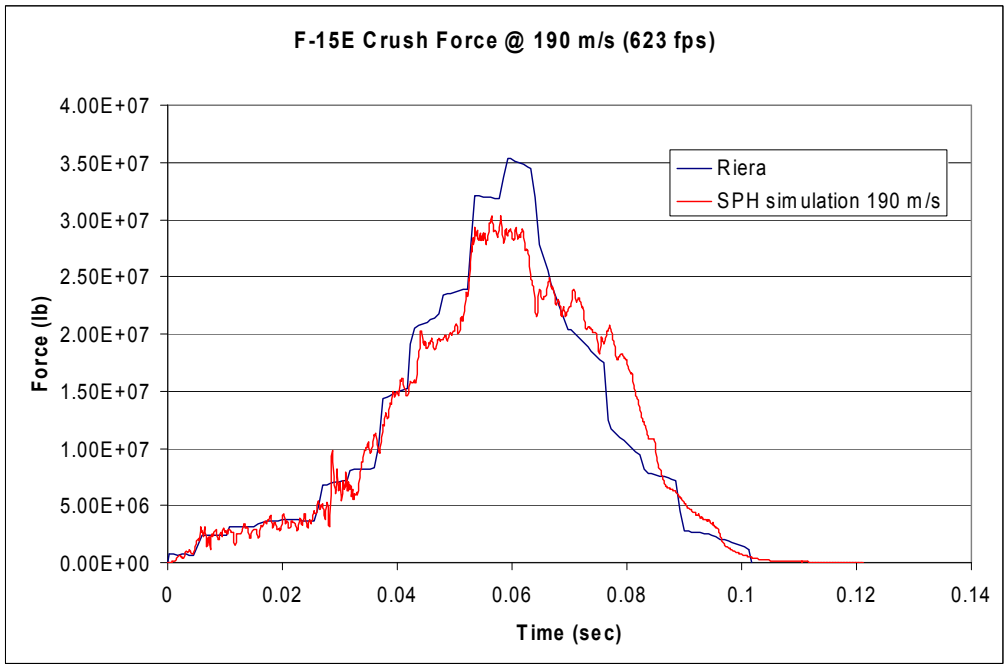

Figure 5-7. Comparison of Impact Forces Calculated by the Riera Method (Riera, 1968) and the SPH Model for an Impact Velocity of 190 m/s [623 ft/s] into a Rigid Surface

impact speed of 112 m/s [367 ft/s] the peak impact force is lower and has an overall impulse that is much lower than the Riera method (Riera, 1968). This can be attributed to the higher speed impact force being dominated by momentum, where material crush strength has less of an effect. The SPH method and the particular mesh used for the skin are not particularly well suited for accurate modeling of bending or crushing. In addition, some of the missing structural components that were lumped in with the skin may have more of an effect on impact forces at the lower speed.

To better match the Riera calculations, some of the material properties of the skin strength and stiffness and the dynamic viscosity of the aircraft fuel were modified through several iterations until better agreement was obtained. The modified parameters included are shown in Table 5-2.

The Young's modulus required a drop of two orders of magnitude before better agreement was established for the lower speed case. Some justification for doing this comes from the methodology used to model the aircraft structure and components. Because all of the internal structure and other major components were lumped in with the weight of the skin, the effective thickness/volume of the skin is much greater than reality. Lowering the skin stiffness is one way to offset this. The dynamic viscosity of the fuel was also increased to obtain better agreement with the Riera method. The results of the rigid wall impact case with the modified parameters are shown in Figures 5-8, 5-9, and 5-10. The additional simulation performed at an impact speed of 215 m/s [705 ft/s] is the same impact speed that was used in the original test of Sugano, et al. (1993). As, noted previously the Riera-calculated impact forces are shown in Figures 5-3 and 5-4.

On the basis of Figures 5-8, 5-9, and 5-10, better agreement is observed using the modified parameters for both speeds. This further emphasizes that the SPH method is better suited for high speed impacts where momentum governs the loading on the wall.

5.3.1 Mesh Sensitivity

A mesh sensitivity study was conducted to determine whether any significant differences in the impact forces on the rigid wall would be observed. Mesh refinement was done on the internal fuel and conformal fuel tanks, and the external fuel tanks were remeshed to improve uniformity, which actually decreased the number of SPH particles in the external tanks by 12,108 SPH particles. Separate models were created with (i) remeshed external tanks and the original mesh for the internal fuel tanks and conformal fuel tanks and (ii) remeshed external tanks and internal and conformal fuel tanks. For both cases, the original mesh for the fuselage was used.

Mesh refinement to the internal and conformal fuel tanks increased the number of fuel SPH particles in the internal tanks by 33,416 particles and number of fuel particles in the conformal fuel tank by 42,480 particles. The fuselage skin was not remeshed, because significant effort was required for its remeshing. However, if major differences were observed by the remeshing of the fuel, a mesh convergence study would be undertaken for the fuselage as well. Also, it was important to keep the total number of SPH particles low enough.

Table 5-2. Final Parameters for Aluminum and Fuel Used in the SPH Model

Aluminum	
Young's Modulus (Pa)	69.0×10^7
Yield Stress (Pa)	40.0×10^6
Fuel	
Dynamic Viscosity (Pa-s)	1.0×10^5

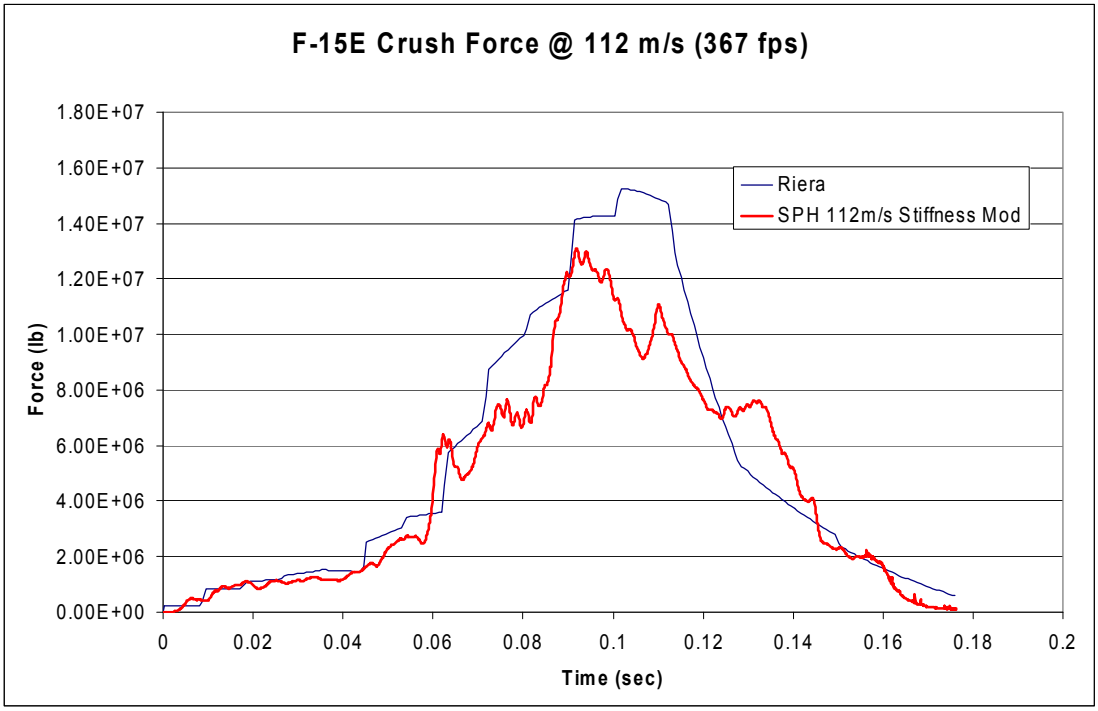

Figure 5-8. Comparison of Impact Forces Calculated by the Riera Method (Riera 1968) and the Revised SPH Model for an Impact Velocity of 112 m/s [367 ft/s] Into a Rigid Surface

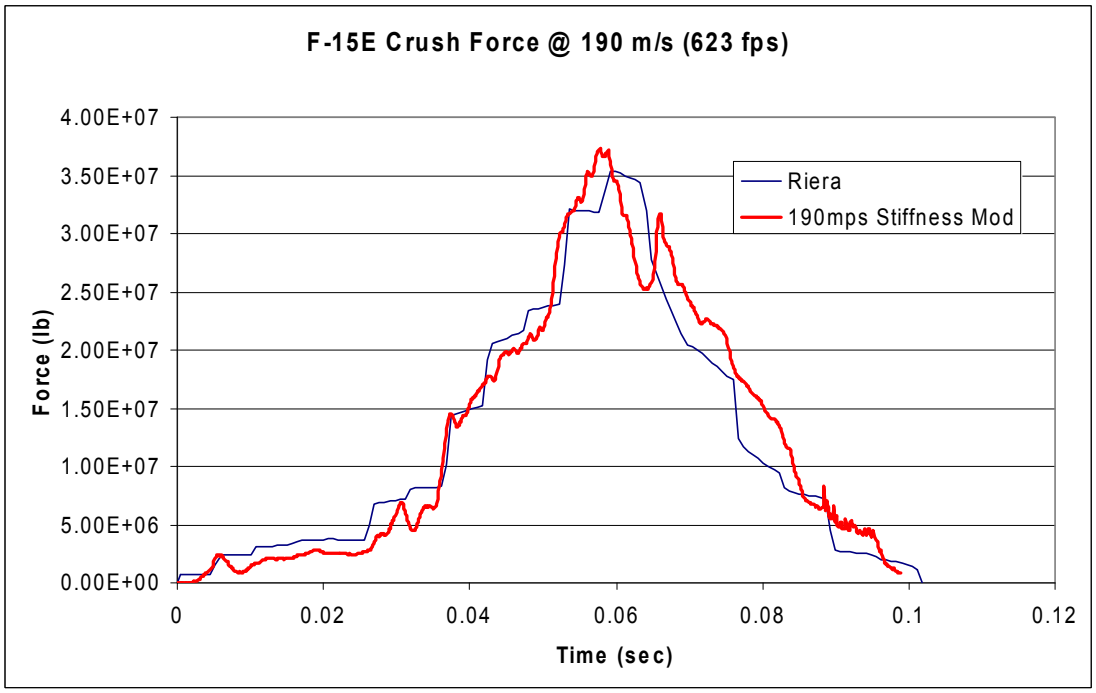

Figure 5-9. Comparison of Impact Forces Calculated by the Riera Method (Riera 1968) and the Revised SPH Model for an Impact Velocity of 190 m/s [623 ft/s] into a Rigid Surface

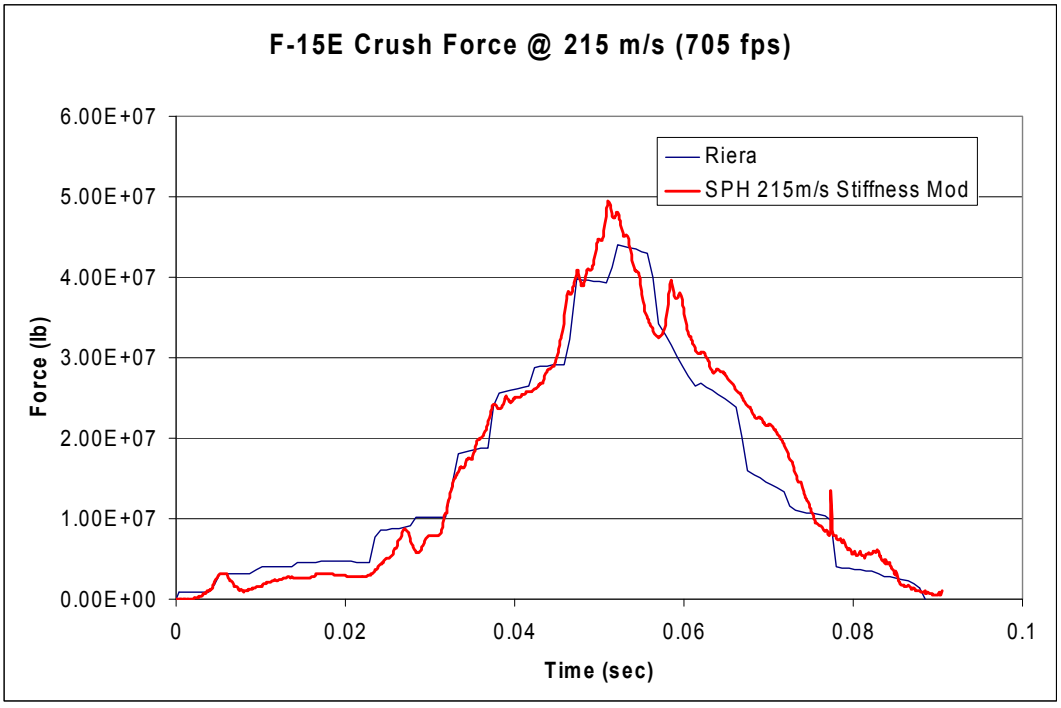

Figure 5-10. Comparison of Impact Forces Calculated by the Riera Method (Riera, 1968) and the Revised SPH Model for an Impact Velocity of 215 m/s [705 ft/s] Into a Rigid Surface

SPH impact simulations could be conducted in a reasonable amount of time and the memory capacity of the computer system would not be exceeded while still achieving accurate results (Figue 5-10).

The SPH model's mass distribution was also refined The mass distribution presented earlier (Figure 4-4) was calculated for 1-m [3.3-ft] increments along the length of the fuselage. However, smaller increments lead to greater variability in the unit mass, even though the total mass and mass distribution of the SPH model has not changed. By varying the increment size, a value of 0.4 m [1.3 ft] gave a similar variability in mass as the F-4 aircraft, as shown by Sugano, et al. (1993).

Figures 5-11 and 5-12 show the distributed mass for the F-15E computed with a 0.4-m [1.3-ft] increment. Figure 5-11 shows the mass distribution for the unrefined SPH mesh, and Figure 5-12 shows the mass distribution using the refined SPH mesh. Comparing Figures 5-11 and 5-12, relatively small differences are apparent. The overall mass of the SPH model has not changed for any of these cases.

For completeness, the crush force for the F-15E aircraft was recomputed using the mass distribution of Figure 5-12 to obtain the values shown in Figure 5-13. Recall that the crush force for the F-15E was scaled from the crush force measured for the F-4 by first scaling by length and then by unit mass. When compared to the initial calculation of the crush force shown in Figure 5-2, determined using the mass distribution in Figure 4-6, the crush force in Figure 5-13 has more variability and a slightly higher peak value. These changes are consistent with the changes in mass distribution between Figures 4-6 {computed for a 1-m [3.3-ft] increment along

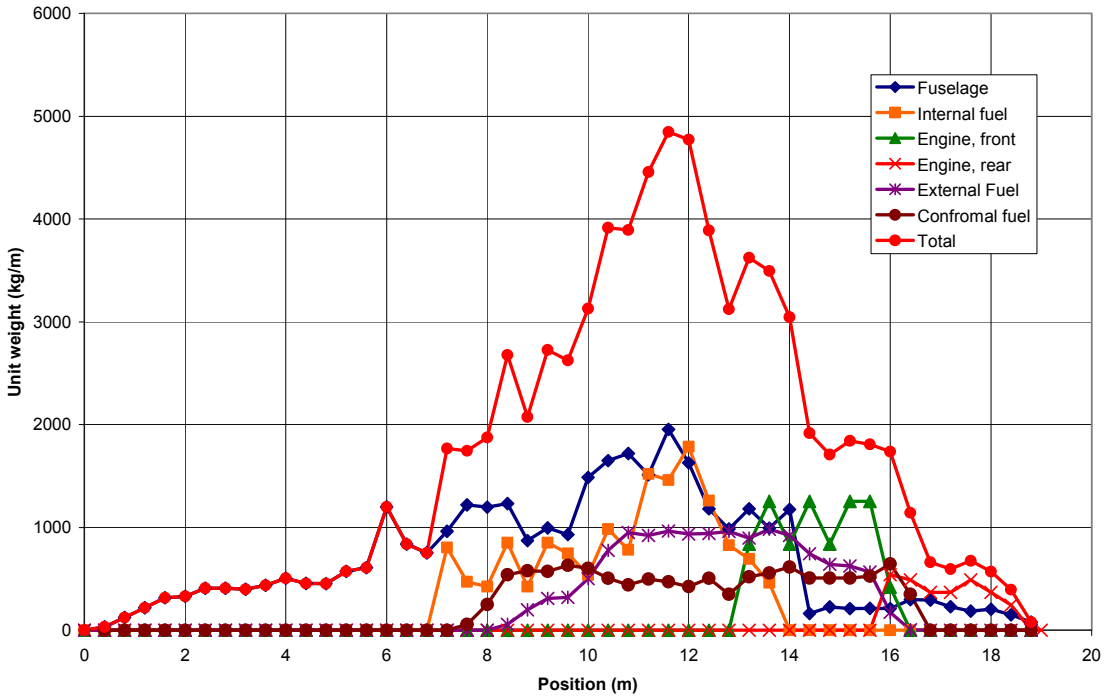

Figure 5-11. Mass Distribution From the Original SPH Model Obtained by Summing the Masses Over 0.4-m [1.3-ft] Increments

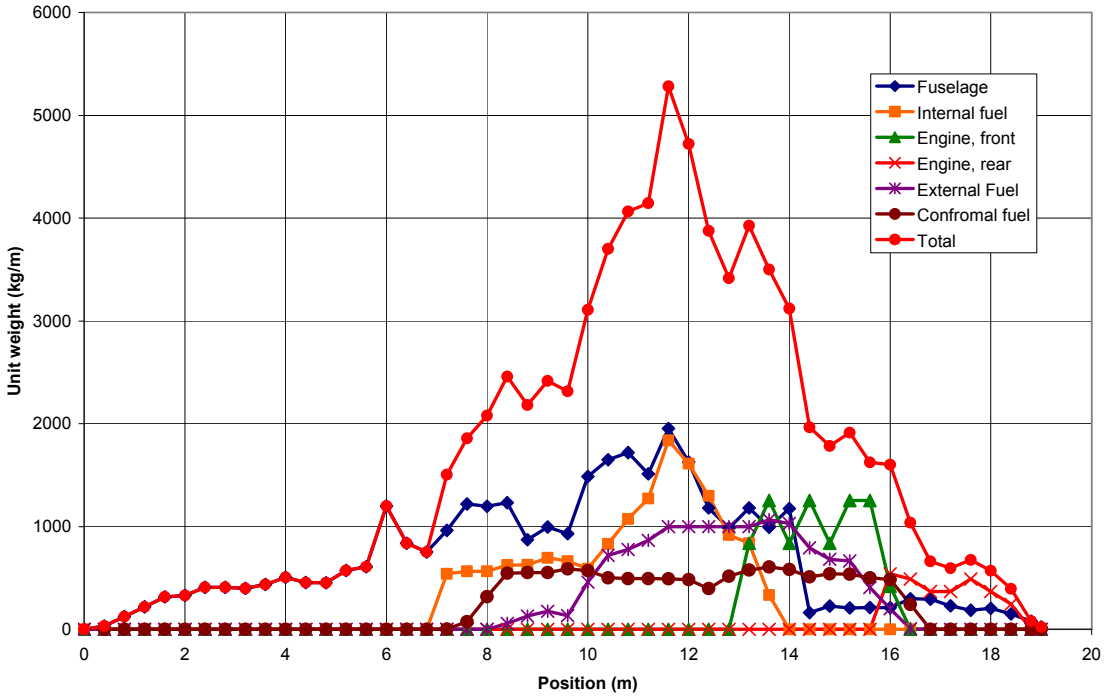

Figure 5-12. Mass Distribution From the Modified SPH Model Obtained by Summing the Masses Over 0.4-m [1.3-ft] Increments

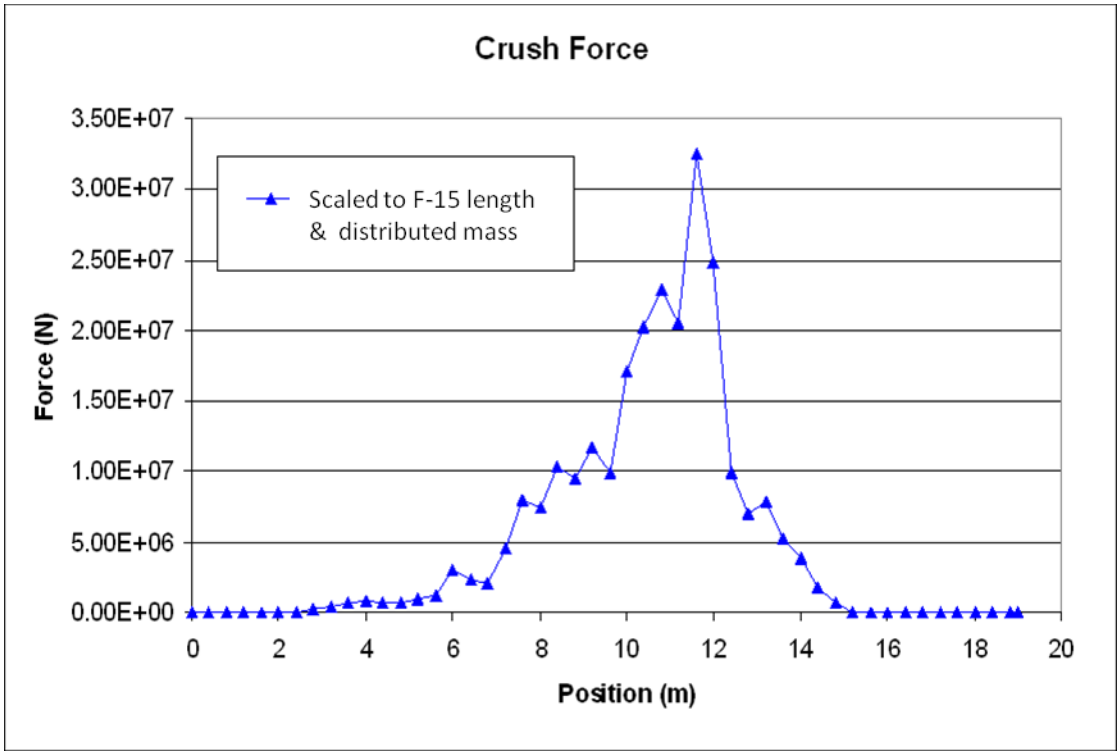

Figure 5-13. F-15E Crush Force Computed from the F-4 Crush Force Using the Mass Distribution of Figure 5-12

the aircraft's length} and Figure 5-12 {computed for a 0.4-m [1.3-ft] increment along the aircraft's length}.

New impact simulations, using the SPH model with the modified fuel mesh, were performed and compared with Riera calculations made using the mass distribution and crush force for the refined mesh computed with a 0.4-m [1.3-ft] increment. Figures 5-14 and 5-15 show the impact forces, computed by the Riera and SPH methods, for impact velocities of 112 and 215 m/s [367 and 705 ft/s], respectively.

Consistent with previous results discussed in Section 5.3, the simulation at the higher impact speed (Figure 5-15) shows the best overall agreement between the SPH model and the Riera method. Figure 5-16 shows a comparison of impact force histories on the rigid wall computed with the SPH model with different meshes. The calculations were performed with the original mesh, the modified fuel mesh, and the modified external tank mesh. The mesh study concluded that no significant differences were observed between the original mesh and modified meshes.

For example, the peak impact forces are higher at some points and lower in others, but overall they are very similar. The small differences are believed to be the result of the refined fuel mesh and how LS-DYNA computes particle interaction (i.e., particle-to-particle contact between different parts). When more fuel particles are included due to mesh refinement, their presence partially slows down the particles used in the rear of the aircraft as it approaches the wall.

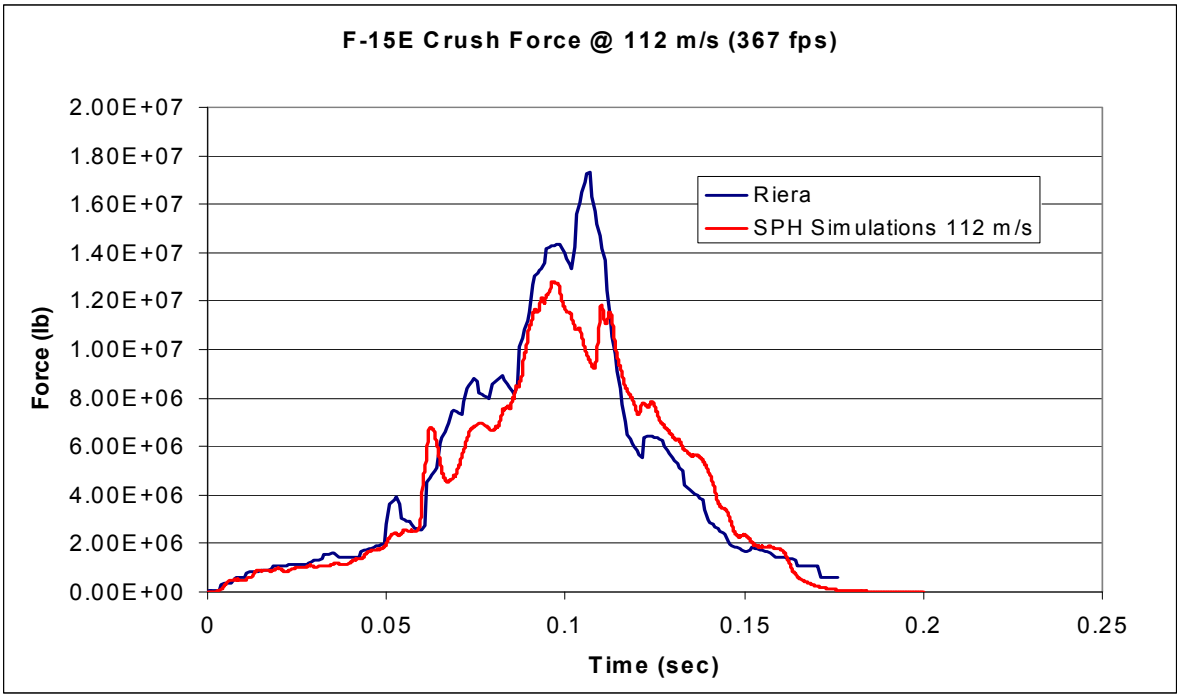

Figure 5-14. Comparison of Impact Forces Calculated by the Riera Method (Riera, 1968) and the SPH Model Using LS-DYNA Version 971 for an Impact Velocity of 112 m/s [367 ft/s]

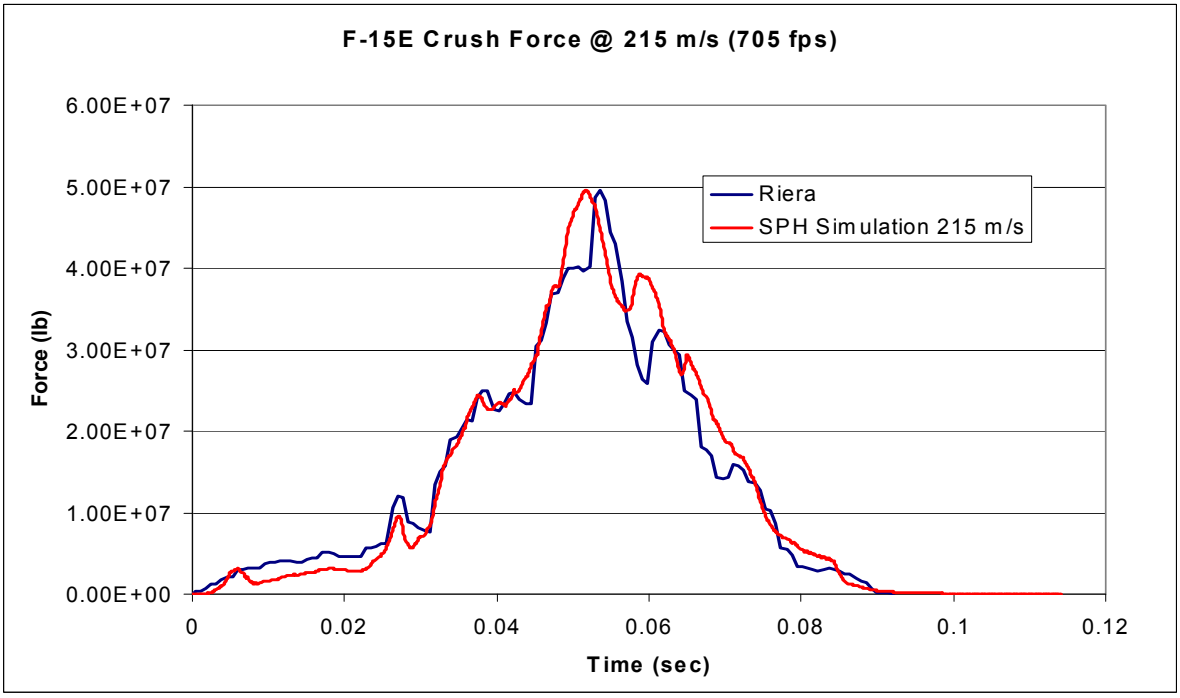

Figure 5-15. Comparison of Impact Forces Calculated by the Riera Method (Riera, 1968) and the SPH Model Using LS-DYNA Version 971 for an Impact Velocity of 215 m/s [705 ft/s]

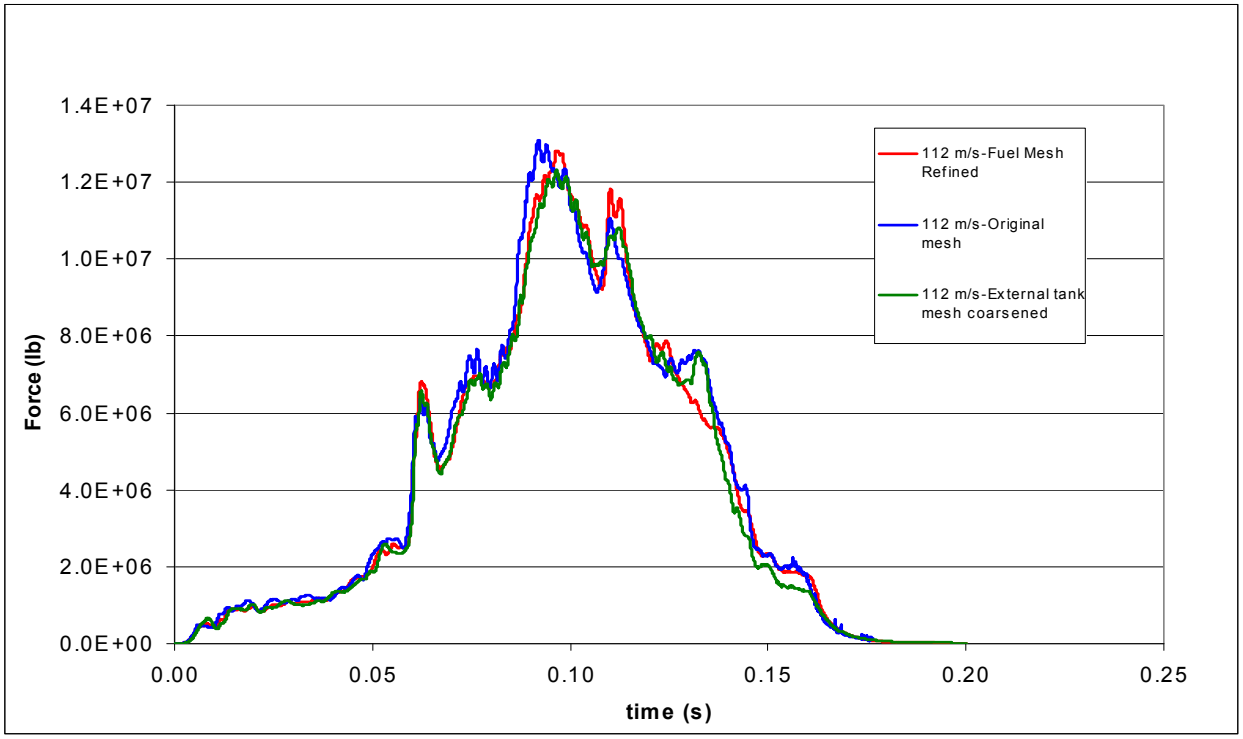

Figure 5-16. The Effect of SPH Model Mesh Refinement on Impact Force Calculated With LS-DYNA Version 971 for an Impact Velocity of 112 m/s [367 ft/s]

Results for higher speed impact cases gave similar results. Note that the simulations used to investigate the fuel mesh refinements were run using LS-DYNA Version 971 due to its release during the course of this work. However, a simulation of the revised external tank mesh was run using both LS-DYNA Versions 970 and 971 to check for any differences and the results are shown in Figure 5-17. Figure 5-17 shows that differences between LS-DYNA Versions 970 and 971 are considered insignificant.

5.3.2 Contact Modeling

One issue that occurred during the impact modeling using the SPH model involved particle contact with solid elements not working properly. It was observed that particles were passing through a wall made of solid elements without interaction as shown in Figure 5-18. If a significant number of particles pass through the wall, not all of the impact energy will be transferred to the structure.

By investigating the different contact options available in LS-DYNA, it was determined that using the SOFT=1 (soft constraint formulation) option worked best for the impact cases being simulated. This option is effective for contact between materials of different stiffness or dissimilar mesh densities (Livermore Scientific Technology Corporation, 2003a).

Another LS-DYNA option used was to invoke a solid element thickness (SLDTHK) for the purpose of contact. This is equivalent to covering the brick elements with null shell elements. To improve computation speed, only the elements with the potential for contact were defined in the segment sets for contact. This can dramatically decrease the computation time required

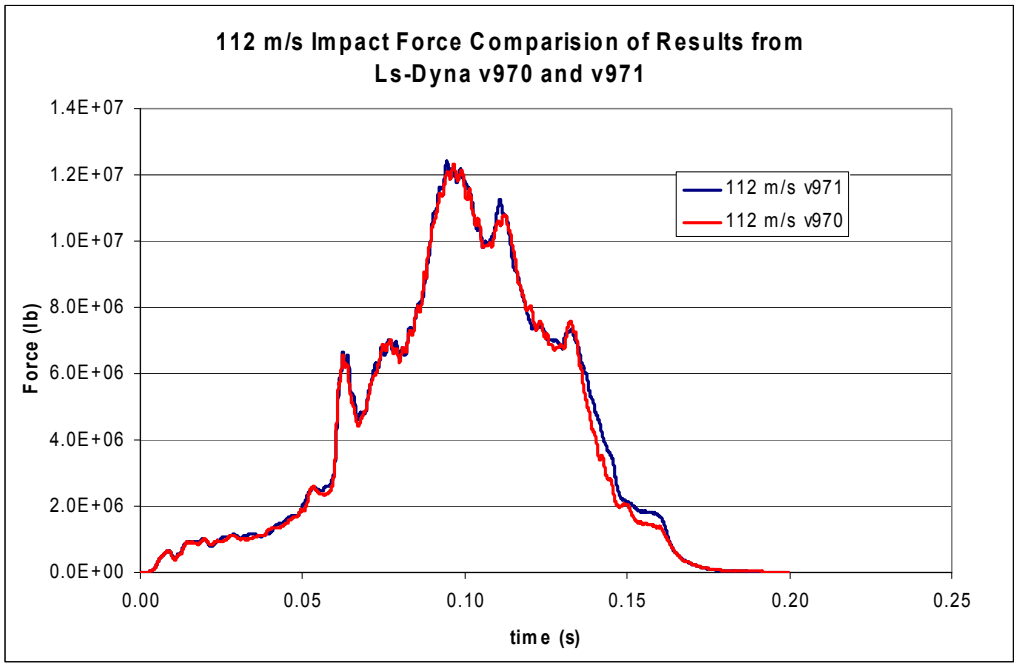

Figure 5-17. Comparison of Impact Forces Calculated with LS-DYNA Versions 970 and 971 for an Impact Velocity of 112 m/s [367 ft/s]

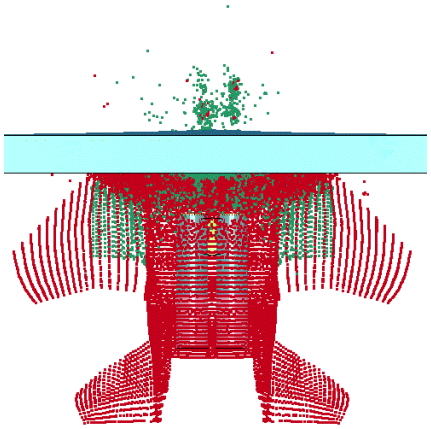

Figure 5-18. Impact Simulation Showing Contact Problem That Allowed SPH Particles of the F-15 Model To Pass Through the Wall

during the contact search algorithms in LS-DYNA. These settings considerably improved the contact situation and minimized the number of particles passing through the solid elements without interaction.

6 FULL-SCALE IMPACT SIMULATION

6.1 Introduction

Chapter 4 discussed the details of constructing the smooth particle hydrodynamic (SPH) model of the F-15E aircraft. Chapter 5 utilized the SPH model to determine the impact forces produced when striking a rigid wall, and comparisons were also made with the impact forces the Riera method (Riera, 1968) calculated. The SPH model underwent a number of refinements to the mesh used for the fuel-related components to improve the match with the Riera-calculated impact forces. Overall, the SPH aircraft model produced good results.

This chapter discusses an impact analysis of the SPH aircraft model striking a reinforced concrete wall.

6.2 Finite Element Modeling of a Reinforced Concrete Wall

The reinforced concrete wall to be modeled consisted of a 76-m [250-ft]-long section with two buttresses spaced equally along its length. Due to the size of the wall, and to allow for a reasonable computation time, only a portion of the wall was modeled. This portion included the two buttresses and the wall between them. An isometric view of the wall and its dimensions are shown in Figure 6-1.

The section of the wall that was modeled was 26.5 m [87 ft] long and 12.2 m [40 ft] high, with a buttress at each end. Specific dimensions of the buttress are shown in Figure 6-1. The wall is 1.2 m [4 ft] thick and has #11 reinforcement steel (rebar) spaced at 30.5 cm [12 in] in both directions with 15.2 cm [6 in] of concrete cover.

The reinforced concrete wall finite element model had a total of 769,904 elements: 704,016 solid elements for the concrete and 65,888 beam elements for the rebar. The rebar beam elements were explicitly defined within the solid elements and shared co-incident nodes.

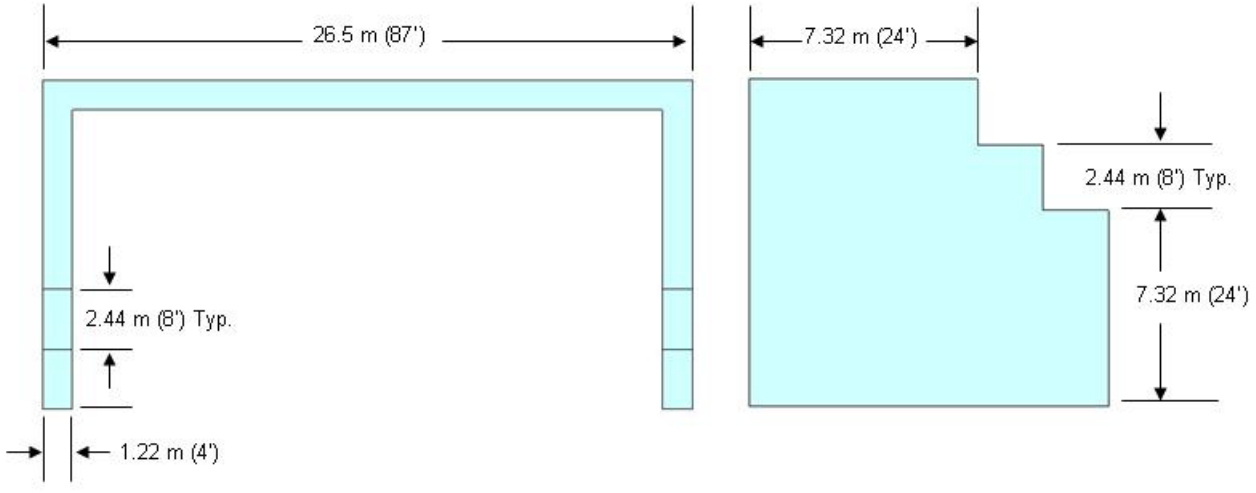

Figure 6-1. Dimensions of the Reinforced Concrete Wall and Buttresses

There were 18 solid elements through the total thickness of the wall, with 3 solid elements to model the thickness of the concrete cover over the rebar. Note that the finite element mesh shown in Figure 6-2 is not uniform and is refined in the area where the aircraft impact will occur. The elements in this area had a discretization interval of approximately 7.6 cm [3 in].

The finite element model of the wall had boundary conditions applied to the top and bottom to account for the contribution due to the intersection of a floor and roof with the wall. Thus the boundary conditions consisted of fixing the translational degrees of freedom along the wall boundary but with free rotation about an axis parallel with the length of the wall.

The concrete material properties used are those given in Section 2. The reinforcement steel (rebar) was modeled using the LS-DYNA *MAT_PLASTIC_KINEMATIC material model, and the properties were consistent for rebar having a yield strength of 414 MPa [60 ksi]. Both the concrete and steel materials used a model for failure based on the effective plastic strain. Once the specified plastic strain value was reached, the element was eroded and no longer included in the calculations.

6.3 Simulation of the F-15E SPH Model Impacting a Reinforced Concrete Wall

This section will discuss the results of the LS-DYNA simulation of the F-15E SPH model impacting the reinforced concrete wall given in Section 6.2.

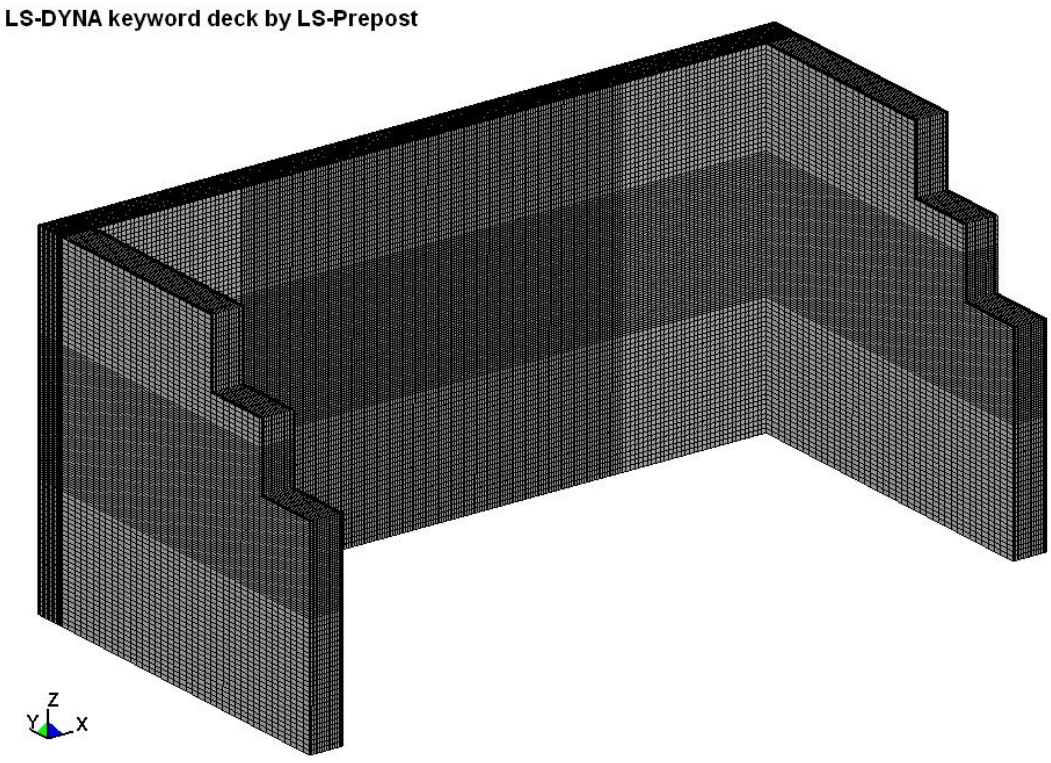

Figure 6-2. Finite Element Model of the Reinforced Concrete Wall and Buttresses

For the following impact simulations, 2 impact speeds were selected based on what was used for the rigid surface impact analysis: 112 and 190 m/s [367 and 623 ft/s]. The aircraft impacted normal to the wall, with the nose directly in the center. The SPH aircraft model used the modified external tank mesh as discussed in Section 5.3.1. Figure 6-3 shows the complete finite element model of the reinforced concrete wall and the SPH aircraft model prior to impact.

Figure 6-4 shows progressive snapshots of the simulation of the aircraft striking the wall at 190 m/s [623 ft/s]. The view of the wall shows the response of the backside of the wall.

The colored contours shown in Figure 6-4 are the effective plastic strain in the concrete elements and are representative of large-scale tensile or shear cracking taking place. Figure 6-5 shows a view from the front of the wall near the end of the simulation. The aircraft has been removed to show the details of the wall. As indicated by the rear and front views, the aircraft has breached the wall. When the simulation was stopped at this point, there still was significant wall motion; therefore, it was expected that large pieces of the wall would continue to break off yielding a larger breach area than shown. During the impact simulation, the wall began to fail as tensile forces caused the rear face rebar to break and concrete elements were deleted due to excessive plastic strain. A major portion of the damage occurred due to the impact of the conformal and internal fuel load, and the wall was breached when the engines struck the wall. Figure 6-6 shows a cut plane view vertically through the center of the wall, when the internal fuel load and engines struck the wall.

A second impact analysis was also performed at an impact speed of 112 m/s [367 ft/s]. Figure 6-7 shows progressive snapshots of the backside of the wall during simulation of the aircraft striking the wall.

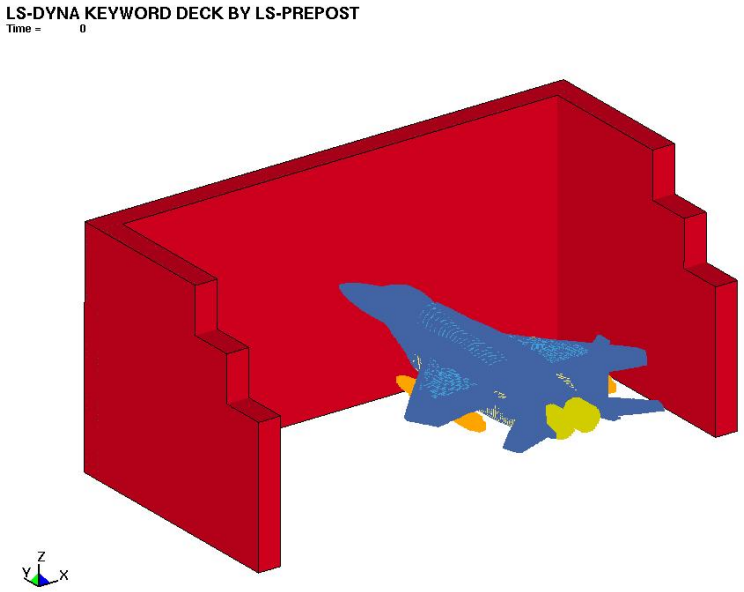

Figure 6-3. Reinforced Concrete Wall and Position of the F-15E SPH Model Just Before Impact

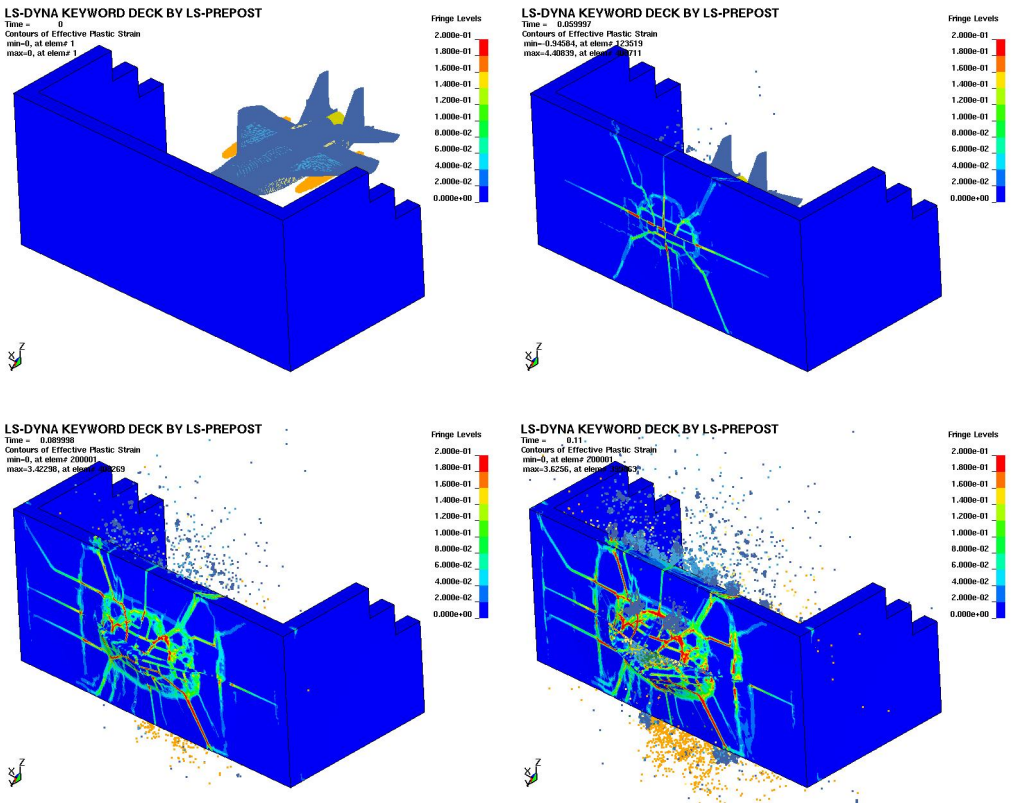

Figure 6-4. Response of the Wall Backside Showing Surface Damage and Contours of Effective Plastic Strain for the F-15E Impact at 190 m/s [623 ft/s]

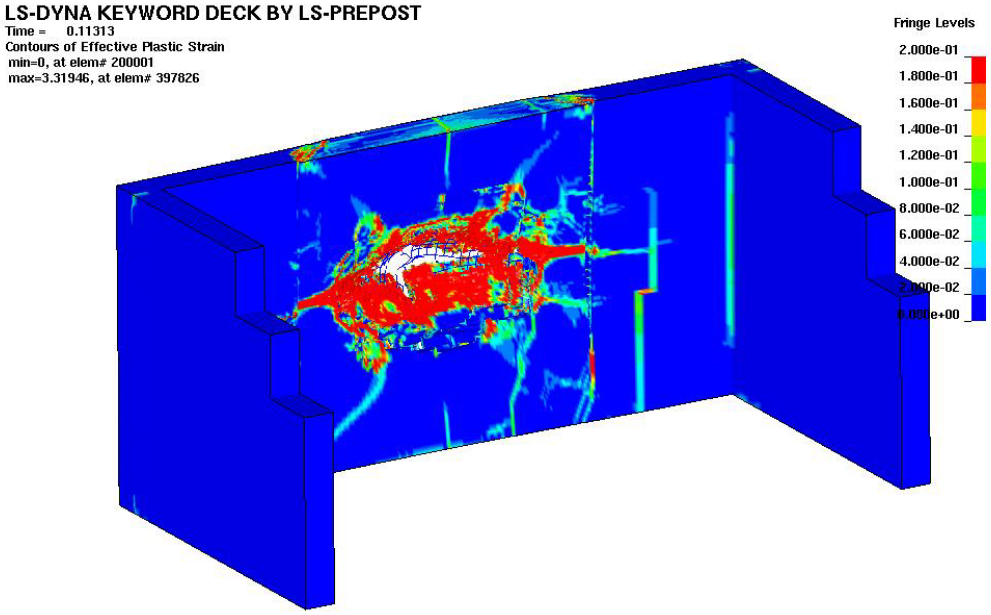

Figure 6-5. Front Face Wall Damage and Contours of Effective Plastic Strain After the F-15E Impact at 190 m/s [623 ft/s]

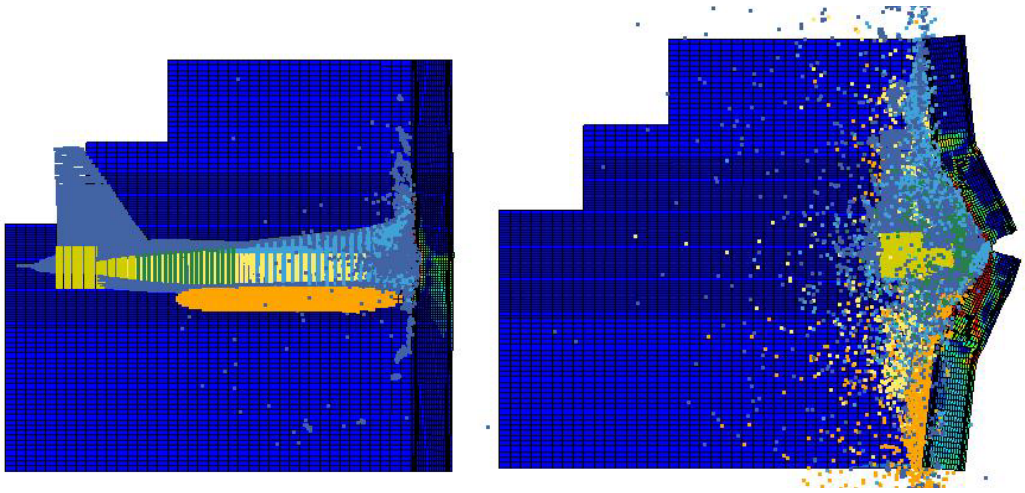

Figure 6-6. Section Through the Wall and F-15E When First External Fuel Tank Reaches the Wall (Left) and When the Engines Contact the Wall (Right) at an Impact Velocity of 190 m/s [623 ft/s]

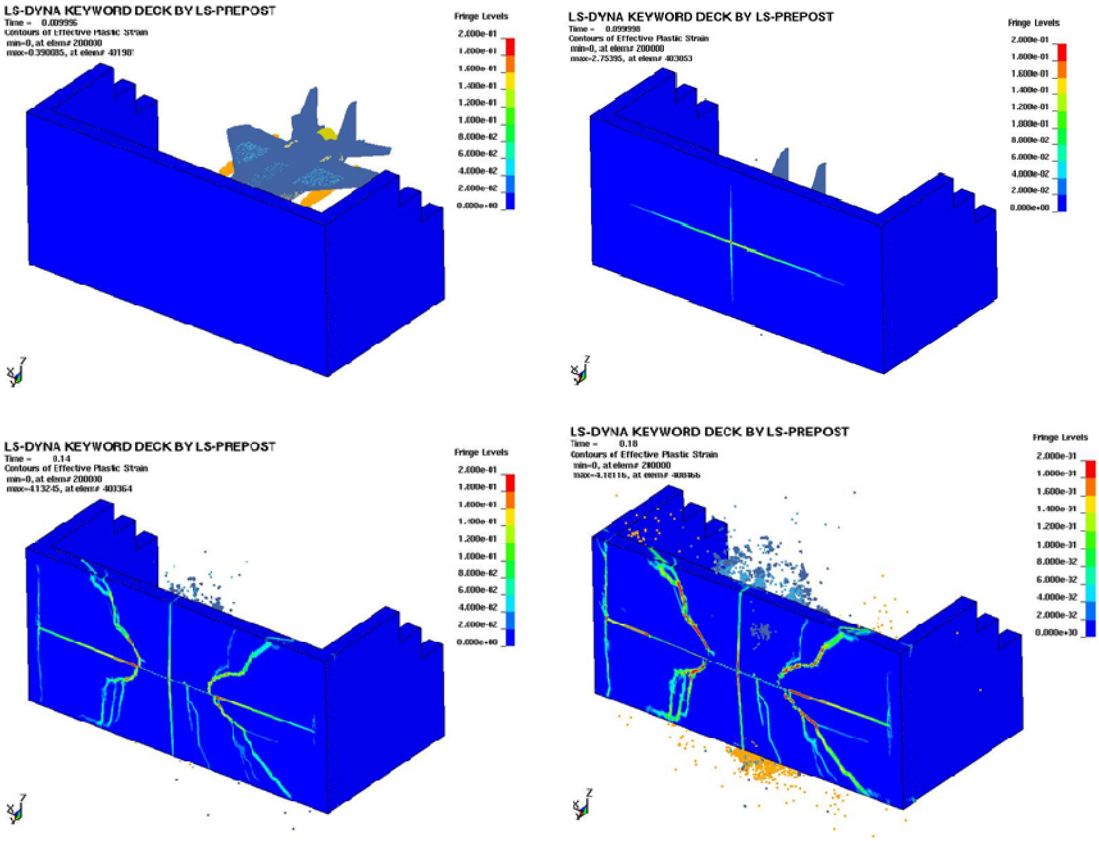

Figure 6-7. Sequence Showing Wall Back Surface Damage and Contours of Effective Plastic Strain for the F-15E Impact at 112 m/s [367 ft/s]

Figure 6-8 shows the final deformed shape of the wall from the front of the wall. For this impact velocity, the wall had not been breached by the aircraft; however, substantial damage was evident from the eroded elements and the distribution of effective plastic strain. Some evidence of possible cracking was indicated by the large plastic strains at the intersection with the buttresses and in the area where the aircraft struck the wall. A displacement time history of a node located at the center of the backside of the wall is shown in Figure 6-9. This time history indicated that the maximum displacement of the wall occurred at 0.2 seconds and had a magnitude of 0.44 m [17 in]. Subsequently, the wall began to spring back and the simulation was stopped because at this point the aircraft model had disintegrated and transferred all of its energy to the wall.

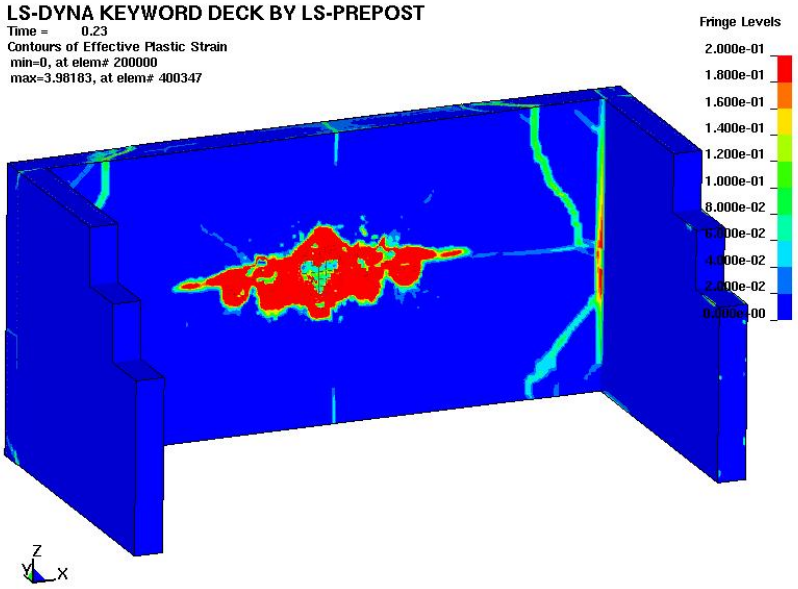

Figure 6-8. Front Face Wall Damage and Contours of Effective Plastic Strain After the F-15E Impact at 112 m/s [367 ft/s]

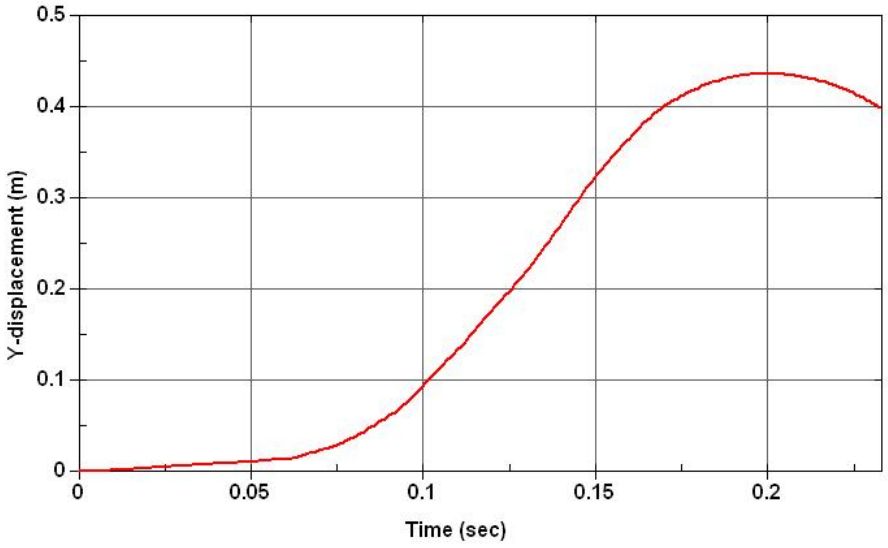

Figure 6-9. Time History of the Wall Back Surface Displacement Located at the Center of Impact of the F-15E at 112 m/s [367 ft/s]

7 SUMMARY AND CONCLUSIONS

7.1 Summary

NRC issued a final rule (74 FR 28111; June 12, 2009) that will require applicants for new power reactors to perform an assessment of the effects on the reactors of the impact of a large, commercial aircraft. As a result, NRC amended 10 CFR Part 50 to include Section 10 CFR 50.150, Aircraft Impact Assessment. Subsequently, NRC issued Draft Regulatory Guide DG–1176 (NRC, 2009), which sets forth a method that NRC considers acceptable for satisfying the regulations in 10 CFR 50.150. NRC has endorsed (NRC, 2009) the use of guidance described in NEI 07-13 (NEI, 2009) as an acceptable methodology for the assessment of aircraft impacts for new nuclear power reactors.

NEI 07-13 (NEI, 2009) states that two structural failure modes need to be evaluated: (i) local failure characterized by scabbing and perforation due to impact of the aircraft engines and (ii) global failure in the form of plastic collapse due to impact of the entire aircraft. One approach for determining both local and global structural failure is the explicit modeling of the aircraft, the target (e.g., a building), and the simulation of the aircraft crashing into the structure. The CNWRA has developed the computational capabilities to perform this type of analysis.

The objective of this report was to present a detailed overview of the work the CNWRA performed as reported by Cox, et al. (2007, 2006, 2005). This CNWRA work was performed under the NRC high-level waste repository safety program. The overall objective of this work was to develop the ability to computationally simulate and analyze the effects of an aircraft crashing into reinforced concrete structures. The structural analysis should evaluate both local and global structurewide responses (NEI, 2009). Thus, two structural failure modes need to be evaluated: (i) local failure characterized by scabbing and perforation due to impact of the aircraft engines and (ii) global failure in the form of plastic collapse due to impact of the entire aircraft.

To achieve this objective, a methodology needed to be developed, which included: (i) selection of the appropriate concrete damage model that was readily available in LS-DYNA, (ii) an accurate characterization of the concrete damage model's material parameters, (iii) a comparison of analytical and numerical methods for calculating the impact force, and (iv) development of an accurate representation of the F-15E aircraft using LS-DYNA.

Chapter 2 discussed the material modeling of concrete. In particular, Section 2.1 presented the LS-DYNA concrete damage model that was used in this study. Among the concrete material models available in LS-DYNA, the concrete damage model based on the formulation of Malvar, et al. (1997) was chosen. The concrete damage model's formulation was thoroughly discussed. The selection of the numerical values for the model's material parameters was based on recommendations given in the LS-DYNA Keyword User's Manual (Livermore Software Technology Corporation, 2003a) and in Malvar, et al. (1997).

To investigate the accuracy of modeling local failure of a reinforced concrete structure, Section 2.2 presented the experimental work of Muto, et al. (1989a,b,c) and Esashi, et al. (1989). These experiments involved impact of small-, intermediate-, and full-scale engine simulants impacting reinforced concrete panels. The engine simulants were based on the GE J79 engine used in the F-4 Phantom fighter aircraft. The experimental results described

the damage to the reinforced concrete panels and the panel's back surface displacement due to the impact.

LS-DYNA simulations were performed using finite element models of the different engine simulants impacting reinforced concrete panels. The results in terms of predicted damage showed very good agreement with the experimental results of Muto, et al. (1989a,b,c) and Esashi, et al. (1989). The agreement between the LS-DYNA numerical simulations and experimental results gave confidence that the initial selection of the material parameters needed for the concrete damage model was appropriate. The displacement time history of the back surface displacement from the LS-DYNA simulation using the full-scale engine simulant matched the measured experimental results in terms of peak displacement. However, it was noted that the bounce back of the reinforced concrete panel was not observed in the LS-DYNA simulation.

Therefore, Section 2.3 presented a sensitivity study to determine specific values of the damage parameters such that the LS-DYNA simulation would also predict the bounce back of the back surface displacement. The results of the study determined values of the damage parameters so that the LS-DYNA simulation results exhibited the bounce back.

However, now the LS-DYNA back surface displacement time history had an unexpected decrease in the displacement rate between approximately 4 and 8 milliseconds . The conclusion was that there appeared to be a coupling between the concrete material parameters and the crush behavior of the LS-DYNA engine simulant and that this required further numerical studies.

Evaluating the accuracy of modeling global structural failure, the force time history analysis method and the missile target interaction analysis method were investigated.

Chapter 3 introduced the force-time history analysis method of Riera. The objective was to study the Riera method (Riera, 1968), which computes the loads imparted to a rigid surface by an aircraft crash. Riera, calculated impact and impulse forces were compared to the experimental data of Sugano, et al. (1993). The results compared favorably to experimentally measured loads of Sugano, et al. (1993). In general, it was found the Riera method would overestimate the impact and impulse forces making the Riera method conservative.

Chapter 4 presented details of the numerical modeling of the F-15E aircraft. Modeling of impact simulations involves large deformations. It is known that the finite element method can have difficulties solving very large deformation problems where significant mesh (element) distortion occurs. Therefore in this report, a mesh-free approach using the SPH method, available in LS-DYNA, was used.

Because limited data were available for the F-15E, the external geometry of the aircraft was constructed from available CAD files. An NRC furnished isometric drawing of the F-15, was used to determine approximate locations of internal components because the drawing was not dimensioned. Using the known weights and location of the aircraft's components, their mass contributions were placed in the external skin of the aircraft. Fuel distribution and information on the aircraft's engines were obtained from various sources. Based upon all of this information, an SPH model of the F-15E aircraft was developed.

In Chapter 5, the impact forces calculated using the Riera method (Riera, 1968) were compared to those produced by the LS-DYNA impact simulation using the SPH model of the F-15E

aircraft. Velocities of 112 and 190 m/s [367 and 623 ft/s] were used in the comparisons. The first comparison indicates that at the lower impact speed of 112 m/s [367 ft/s], the LS-DYNA simulation produces a peak impact force that is 33 percent lower than the impact force the Riera method calculated. This may be due the crush force (i.e., structural stiffness) of the aircraft having a significant effect on the impact force. The second comparison shows that for the impact speed of 190 m/s [623 ft/s], the impact force from the LS-DYNA simulation is 4 percent lower than the impact force the Riera method (Riera, 1968) calculated. The better agreement with the Riera calculation at the higher impact velocity may be due to the dominance of the inertial force with the differences in crush force becoming less significant.

Finally, Chapter 6 used the missile target interaction analysis method to model the global failure of a reinforced concrete wall. The impact into a reinforced concrete wall was simulated using the LS-DYNA SPH model of the F-15E aircraft. At an impact velocity of 112 m/s [367 ft/s], considered as low, the wall withstands the impact but suffers damage. At a 190-m/s [623-ft/s] impact velocity, the model predicts significant damage with the wall being breached.

7.2 Conclusions

The assessment of commercial and military aircraft crash hazards and their impact on nuclear and other critical facilities are important to the owners of these facilities and many federal government agencies. Based on the results summarized previously on the work the CNWRA performed for NRC high-level waste repository program, some conclusions have been made regarding the effectiveness of the methodology developed for simulation of the response of reinforced concrete structures due to aircraft crash impact.

Application of the concrete damage model for impact simulations using idealized aircraft engine models striking reinforced concrete panels matched experimentally observed damage modes. However, the panel's back surface displacements did not capture the observed bounce-back behavior. Attempts were made to adjust the concrete damage material parameters to capture the bounce-back behavior. By performing a sensitivity study, the bounce-back behavior was captured; however, these adjustments to the concrete material parameters resulted in an offset in the LS-DYNA calculated displacement time history.

A second sensitivity study to further investigate the displacement offset was performed, in which material parameters used in the LS-DYNA engine simulant model were varied. Based on the results of the sensitivity study, it was determined that the offset in the displacement time history was also affected by the collapse of the front cylinder of the LS-DYNA engine simulant model.

The conclusion is that there appears to be a coupling between the concrete material parameters and the crush behavior of the LS-DYNA engine simulant. This conclusion is important because it demonstrates that the global response of the concrete structure is affected not only by the concrete material behavior, but also by the crush behavior of the engine. Therefore, it is recommended that additional numerical studies be performed to further investigate this apparent coupling and its effect on the structure's displacement time history.

Lack of data affects the use of the force-time history (i.e., Riera) method because it requires the mass distribution and the crush force along the length of the aircraft. In this current study, when the Riera (Riera, 1968) method was used to calculate the impact force for the F-15E aircraft, the required crush force was scaled from the F-4 aircraft crush force Sugano, et al. (1993) provided. This was considered acceptable because the F-15E is similar in size and weight to the F-4 aircraft. Therefore, a possible limitation using the Riera method is the availability of mass

distribution and fuselage crush strength data. Hossain, et al. (1997) also noted this limitation. The development of the F-15E SPH model was also difficult due to lack of data. An isometric drawing of the F-15 provided only an approximate location of the internal components, and the F-15E's mass distribution had to be scaled from the known mass distribution of the F-4.

Therefore, using either the force-time history or missile target interaction method to perform a realistic aircraft impact assessment using a commercial aircraft would require sufficiently detailed data. However, obtaining this data from an aircraft manufacturer may be difficult, as it is usually proprietary information.

The use of the SPH method to model the aircraft can be considered a somewhat novel approach. In this report, the SPH method was shown to provide an alternative to the finite element method for performing impact crash analysis. However, its use may only be appropriate when the inertial force is dominant (i.e., high velocity impact where the crush strength has less of an effect). As shown in Figure 5-7, at an impact velocity of 112 m/s [367 ft/s] the SPH model produced a significantly lower peak impact force as compared to the Riera method (Riera, 1968). Thus it was concluded that at low velocities, the bending, buckling, or crushing of the fuselage may become significant.

Although this report focused on reinforced concrete structures, the same methodology can be applied to other structures that may be constructed of steel only or a combination of both steel and reinforced concrete. Accurately modeling the behavior of steel would be straightforward because constitutive models for metals that include high strain rate effects, temperature dependence, and failure criteria are well established.

Additional technical issues not covered in this report that are important to address are (i) shock and vibration analysis of the complete structure and (ii) the evaluation of fire effects to determine the extent of structural damage due to possible spread of aviation fuel. For example, as the NIST study of the WTC terrorist attack determined, fire caused steel trusses to fail, which played a significant part in the structural collapse of the towers.

As documented in this report, a significant amount of work has been accomplished in establishing a methodology for the simulation of the response of reinforced concrete structures due to aircraft crash impact.

The experience gained from these studies will be useful for performing aircraft impact assessments for reinforced concrete structures of geologic repositories and other critical facilities.

8 REFERENCES

74 FR 28111. "Consideration of Aircraft Impacts for New Nuclear Power Reactors: Final Rule." *Federal Register*. Vol. 74, No 112. pp. 28111–28143. June 12, 2009.

Aerospaceweb.org. "McDonnell Douglas (now Boeing) F-15E Eagle Fighter Bomber. 2011. <http: //www.aerospaceweb.org/aircraft/bomber/f15e.> (March 20, 2011).

Chen, W.F. *Plasticity in Reinforced Concrete*. Fort Lauderdale, Florida: J. Ross Publishing, Inc. 2007.

Cox, P.A., J. Mathis, T. Wilt, and A. Chowdhury. "Assessment of Structural Robustness Against Aircraft Impact at the Potential Repository at Yucca Mountain—Progress Report III." San Antonio, Texas: CNWRA. July 2007.

Cox, P.A., J. Mathis, T. Wilt, A. Chowdhury, and A. Ghosh. "Assessment of Structural Robustness Against Aircraft Impact at the Potential Repository at Yucca Mountain—Progress Report II." San Antonio, Texas: CNWRA. September 2006.

Cox, P.A., J. Mathis, and A. Ghosh. "Assessment of Structural Robustness Against Aircraft Impact at the Potential Repository at Yucca Mountain—Progress Report." San Antonio, Texas: CNWRA. August 2005.

Esashi, Y., H. Ohnuma, C. Ito, and K. Shirai. "Experimental Studies on Local Damage of Reinforced Concrete Structures by the Impact of Deformable Missiles, Part 2: Intermediate-Scale Tests." Transaction of the 10th International Conference on Structural Mechanics in Reactor Technology (SMiRT 10), Anaheim, California, August 14–19, 1989. Los Angeles, California: American Association for Structural Mechanics in Nuclear Reactors. 1989.

Hossain, Q.A., R.P. Kennedy, R.C. Murray, K. Mutreja, and B.P. Tripathi. "Structures, Systems, and Components Evaluation Technical Support Document. DOE Standard, Accident Analysis for Aircraft Crash into Hazardous Facilities." UCRL–ID–123577. Livermore, California: Lawrence Livermore National Laboratory, United States Department of Energy. 1997.

Livermore Software Technology Corporation. "LS-DYNA Keyword Users Manual." Version 970. Livermore, California: Livermore Software Technology Corporation. April 2003a.

Livermore Software Technology Corporation. "LS-DYNA Theory Manual." Version 970. Livermore, California: Livermore Software Technology Corporation. April 2003b.

Livermore Software Technology Corporation. "LS-PrePost Software." April 2003c. <http: //www.lstc.com/lsprepost.htm>. Livermore, California: Livermore Software Technology Corporation. (January 1, 2011)

Malvar, L.J., J.E. Crawford, J.W. Wesevich, and D. Simons. "A Plasticity Concrete Material Model for DYNA3D." *International Journal of Impact Engineering*. Vol. 19, Nos. 9–10. pp. 847–873. 1997.

Microsoft® Corporation. "Microsoft Excel 2002.5P3." Redmond, Washington: Microsoft Corporation. 2002.

Muto, K., H. Tachikawa, T. Sugano, H. Tsubota, H. Kobayashi, Y. Kasai, N. Koshika, and T. Tsujimoto. "Experimental Studies on Local Damage of Reinforced Concrete Structures by the Impact of Deformable Missiles, Part 1: Outline of the Test Program and Small-Scale Tests." Transaction of the 10th International Conference on Structural Mechanics in Reactor Technology (SMiRT 10), Anaheim, California, August 14–19, 1989. Los Angeles, California: American Association for Structural Mechanics in Nuclear Reactors. 1989a.

Muto, K., H. Tachikawa, T. Sugano, H. Tsubota, N. Nagamatsu, N. Koshika, M. Okano, K. Suzuki, and S. Ohrui. "Experimental Studies on Local Damage of Reinforced Concrete Structures by the Impact of Deformable Missiles, Part 3: Full-Scale Tests." Transaction of the 10th International Conference on Structural Mechanics in Reactor Technology (SMiRT 10), Anaheim, California, August 14–19, 1989. Los Angeles, California: American Association for Structural Mechanics in Nuclear Reactors. 1989b.

Muto, K., T. Sugano, H. Tsubota, N. Koshika, Y. Esashi, H. Ohnuma, and C. Ito. "Experimental Studies on Local Damage of Reinforced Concrete Structures by the Impact of Deformable Missiles, Part 4: Overall Evaluation of Local Damage." Transaction of the 10th International Conference on Structural Mechanics in Reactor Technology (SMiRT 10), Anaheim, California, August 14–19, 1989. Los Angeles, California: American Association for Structural Mechanics in Nuclear Reactors. 1989c.

Nuclear Energy Institute (NEI). "Methodology for Performing Aircraft Impact Assessments for New Plant Designs, Revision 7." NEI 07-13. Washington, DC: Nuclear Energy Institute. May 2009.

NRC. "Guidance for the Assessment of Beyond-Design-Basis Aircraft Impacts." DG–1176. Washington, DC: NRC. 2009.

NRC. NUREG–0800, "Standard Review Plan for the Review of Safety Analysis Reports for Nuclear Power Plants." Washington, DC: NRC. June 1987.

Pratt and Whitney. "F100–PW–229 Engine Enhancement Package." 2011. East Hartford, Connecticut: Pratt and Whitney. <http: //www.pw.utc.com> (06 June 2011).

Riera, J.D. "On the Stress Analysis of Structures Subjected to Aircraft Crash on Building Structures." *Nuclear Engineering and Design*. Vol. 8. pp. 415–426. 1968.

Sugano, T., H. Tsubota, Y. Kasai, N. Koshika, S. Orui, W.A. von Riesemann, D.C. Bickel, and M.B. Parks. "Full-Scale Aircraft Impact Test for Evaluation of Impact Force." *Nuclear Engineering and Design*. Vol. 140. pp. 373–385. 1993.

XYZ Scientific Applications, Inc. "TrueGrid." Livermore, California: XYZ Scientific Applications, Inc. 2006.